Submicron-Sampling of Living Cells by Macrophages

Authors: Amy C. Fan[1,‡], Rukman Thota[1,2], Nina Serwas[1,3], Vivasvan S. Vykunta[1,2,4], Kyle Marchuk[5], Megan K. Ruhland[1,6], Lauren Liu[1], Grace Johnson[1], Austin Edwards[5], Matthew F. Krummel[1,‡]

---

[1]Department of Pathology, University of California San Francisco, San Francisco, CA, USA.

[2]Biomedical Sciences Graduate Program, University of California San Francisco, San Francisco, CA, USA

[3]Current Address: Arcus Biosciences, Hayward, CA, USA

[4]Medical Scientist Training Program, University of California San Francisco, San Francisco, CA, USA

[5]Parnassus Advanced Light Microscopy CoLab, University of California, San Francisco, CA, USA.

[6]Current Address: Department of Cell, Developmental & Cancer Biology, Oregon Health & Science University, Portland, OR, USA

[‡]Lead Contacts, email: amy.fan@ucsf.edu, matthew.krummel@ucsf.edu

SUMMARY PARAGRAPH

An effective immune system must sample and appreciate healthy-self identity to prevent autoimmunity and to contrast to pathogenic insults[1–3]. Self-proteins are presented to T cells in the thymus during immune cell development[2,3], and must be presented throughout the body to both maintain regulatory T cell populations[4–6] and provide a tonic signal to maintain conventional T cells over time[7–9]. The ready observations of continuous apoptosis in some organs together with the ingestion of that material by myeloid populations has led to a conventional understanding of ongoing cell-death as a major source of self-antigens[10], complemented in some situations by uptake of free-floating cell-derived vesicles. Here, we used a series of companion imaging and vesicular labeling technologies to reveal an alternate process undertaken by macrophages that results in non-destructive and direct sampling of living cells. The process requires cell-cell contact, does not require caspase activation, and takes place via a trogocytosis-like stretching of the target cell into the macrophage, leading to the generation of submicron-sized vesicles containing cytoplasm. Using a high-dimensional flow-based method for labeling vesicles ingested under this versus other conditions, we find that live-sampled material is distinctly processed, is poorly subject to fusion with lysosomes, and produces ensuing differential effects on the presentation of those to CD4 versus CD8 T cells. Disrupting this trafficking by redirecting antigen to the lysosome significantly reduced the associated macrophage-mediated priming of CD8 T cells. This demonstrates an important and substantial sampling of living cells by the immune system, with clear consequences for maintaining the border of immunity.

43 **MAIN**

44 **Tissue and tumor-associated proteins are routinely sampled by myeloid cells**

45 Antigen presenting cells (APCs) must continuously survey tissues by ingesting and processing antigens for
46 presentation to direct antigen-specific T cell responses[11]. In the course of studying a selection of tissue-
47 specific sites of tolerance, including in tumors, we expressed the fluorescent protein ZsGreen in multiple
48 non-inflammatory settings across a range of tissues with slow turnover rates (Scbg1a1-Cre-ERT2; airway
49 epithelium)[12] or faster turnover (K14-Cre skin, tumors, Villin-Cre intestinal epithelium). ZsGreen is both
50 bright and very stable, permitting superior long-lived tracking[1,10,24]. Cytosolic ZsGreen expressed under
51 these promoters all routinely illuminated substantial $CD45^+$ immune populations that contained numerous
52 submicron-sized vesicular puncta of ZsGreen (**Fig. 1a, b)**, consistent with ingestion of tissue-associated
53 protein. When $CD45^+$ cells bearing $ZsGreen^+$ were isolated from these healthy tissues, a variety of myeloid
54 cells were highlighted (**Fig. 1c, d; Extended Data Fig. 1a,b; Supplementary Fig. 2**), including dendritic
55 cells and neutrophils but with macrophages being the most consistently loaded. These loading frequencies
56 also mirror previous characterization of myeloid sampling of skin[13] and tumor cytoplasts[14].

57

58 These observations do not result from misexpression of transgenes in host tissues as demonstrated by the
59 following series of observations. First, we compared the ZsGreen fluorescence intensity of lung myeloid
60 cells in mice expressing ubiquitous ZsGreen ("B-actin-Cre;ZsGreen"), lung-specific ZsGreen ("Scgb1a1-
61 Cre-ERT2;ZsGreen"), or no ZsGreen (C57BL/6 wildtype, "B6 WT"). In each myeloid cell population,
62 ZsGreen fluorescence intensity in the Scgb1a1-Cre-ERT2;ZsGreen mice was greater than in B6 WT mice
63 but less than in B-actin-Cre;ZsGreen mice (**Extended Data Fig. 1b**), consistent with accumulation of
64 exogenous ZsGreen protein as opposed to cell-autonomous ZsGreen expression. Second, normal bone-
65 marrow transplanted into mice expressing ZsGreen gave rise to donor-derived myeloid cell populations that
66 were bright for ZsGreen (**Extended Data Fig. 1c; Supplementary Fig. 3a**). Third, in mice ubiquitously
67 expressing TdTomato transplanted subcutaneously with B16F10 tumors expressing ZsGreen ("B16-

ZsGreen"), host CD45^{+} immune cells contained tumor-derived vesicular ZsGreen puncta and a significant proportion of tumor-associated myeloid cells ingested ZsGreen (**Fig. 1e,f, Supplementary Fig. 3b**). Finally, whereas we had previously observed trafficking of tissue-specific ZsGreen to tissue draining lymph nodes[13], ZsGreen was not detected in the non-draining lymph node of Scgb1a1-Cre-ERT2;ZsGreen mice (**Fig. 1g**), indicating tissue-specific uptake.

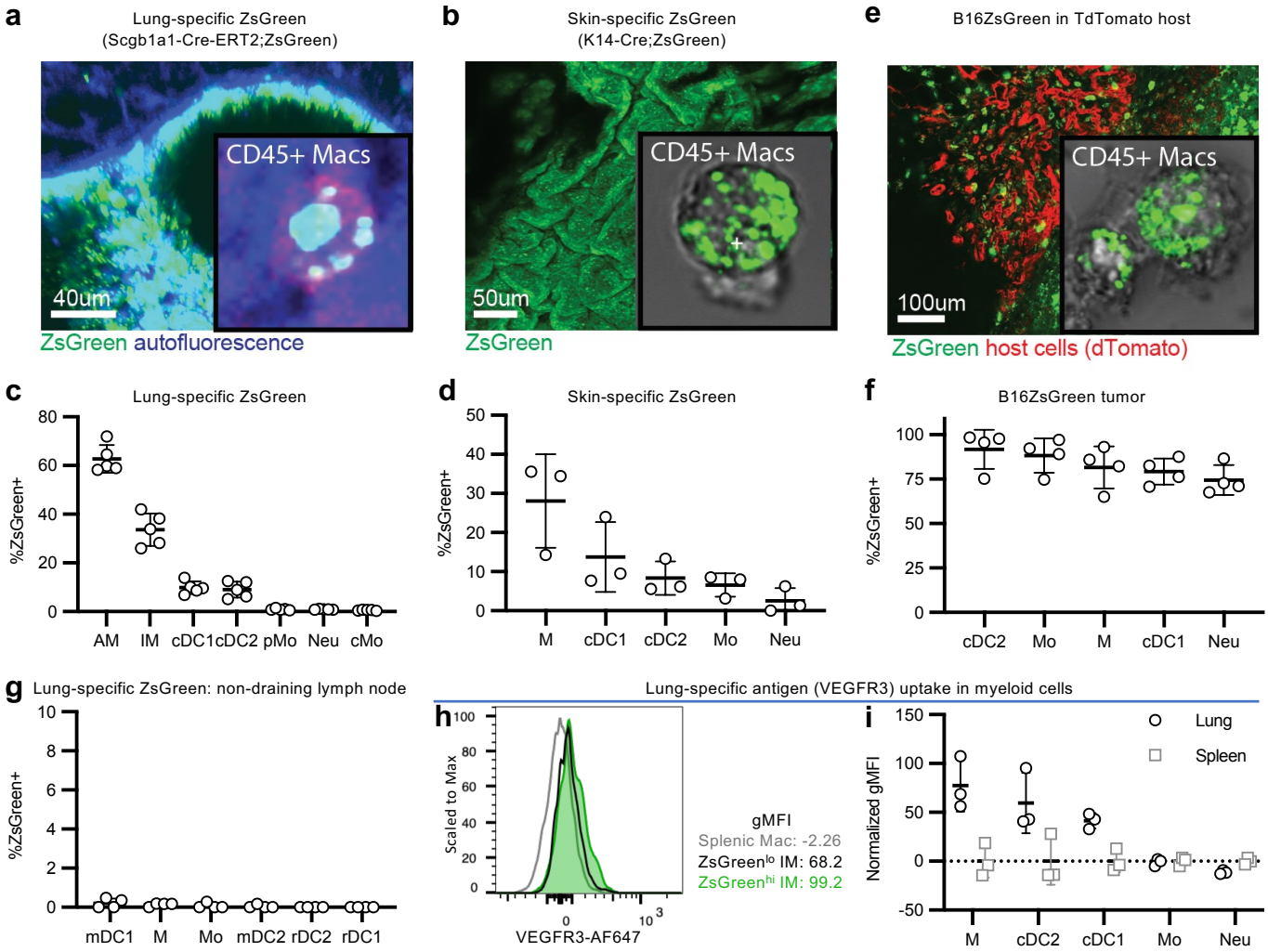

Figure 1: Myeloid cells sample proteins from healthy and tumor tissues

a-b, Lungs (**a**) or skin (**b**) taken from mice expressing ZsGreen under the Scgb1a1 (**a**) or K14 (**b**) Cre with insets of in situ macrophages labeled with CD45 (**a**) or sorted CD45+ Macrophages (**b**) showing ZsGreen puncta inside macrophages. **c-d,** Isolation of lung myeloid cells from Scgb1a1-Cre-ERT2;ZsGreen mice (**c**) or skin myeloid cells from K14-Cre;ZsGreen mice (**d**) shows specific uptake in tissues prominently in macrophages. Lymphocytes were routinely ZsGreen negative. **e,** B16 melanoma cells expressing ZsGreen transplanted into mice ubiquitously expressing TdTomato with inset of CD45+ macrophages. **f**, Isolation of tumor-associated myeloid cells shows broad uptake of ZsGreen across myeloid cell subsets. **g**, Isolation of inguinal LN myeloid cells from Scgb1a1-Cre-ERT2;ZsGreen mice shows no uptake in distant lymph nodes. **h,** Intracellular staining for airway specific VEGFR3 protein in lung (black) compared to splenic (gray) myeloid cell populations with ZsGreen^{hi} lung macrophages (green) further enriching for VEGFR3 signal. **i,** VEGFR3 MFI in lung and splenic myeloid cell populations normalized to average MFI of splenic myeloid cells. Representative of 3 experiments, n = 3-6 mice per experiment. AM, alveolar macrophage; IM, interstitial macrophage; pMo, patrolling monocyte; Neu, neutrophil; cMo, conventional monocyte; M, macrophage; Mo, monocyte, mDC2, migratory cDC2; mDC1, migratory cDC1; rDC1, residential cDC1; rDC2, residential cDC2

88 For tumor antigens, it was previously found that tumor antigens were co-packaged in macrophage vesicles,
89 together with tumor-derived ZsGreen tracer[13]. To determine if other non-tumor self-antigens in healthy
90 tissues with low turnover like epithelium were similarly taken up in these myeloid cell populations, we
91 examined the levels of VEGFR3 and PLVAP proteins, which are specifically expressed on the cell surface
92 of non-hematopoietic cells in the lung. When we examined the cellular components from the lungs of
93 Scgb1a1-Cre-ERT2;ZsGreen mice by intracellular flow-cytometry, we found that local myeloid cell
94 populations from the lung, but not distant splenic myeloid cells, contained these self-proteins **(Fig. 1h, i;**
95 **Extended Data Fig. 1d; Supplementary Fig. 3c)**. Further, ZsGreen^{hi} myeloid cells were brighter for the
96 VEGFR3 and PLVAP stains as compared to ZsGreen^{lo} myeloid cells (**Fig. 1h; Extended Data Fig. 1d**).
97 Therefore, tissue-associated myeloid cells regularly sample tissue-associated self-proteins, both normal and
98 tracer.
99

100 **Substantial antigen sampling from live cells by macrophages**

101 Several mechanisms of uptake might contribute to myeloid cell sampling from tissues in vivo, with the most
102 heavily studied to date being phagocytosis of dead cells and endocytosis of exosomes. To formally
103 interrogate how myeloid cells can obtain intracellular material from nearby cells, we established an in vitro
104 assay for sampling using donor cell populations, grown at ~99% viability, in log phase. We co-cultured
105 bone marrow derived macrophages (BMDMs) with those ZsGreen-expressing target, especially focusing
106 on two model target cells: B16-ZsGreen melanoma cells which in these conditions minimally produce
107 exosomes, or primary mouse embryonic fibroblasts isolated from mice ubiquitously expressing ZsGreen
108 ("MEF-ZsGreen"). From this co-culture, we detected significant ZsGreen^{+} uptake from both target cells
109 into the BMDM, with the intensity of that ZsGreen being hundreds of times lower than the intensities of
110 intact donor cells, consistent with partial sampling as opposed to complete engulfment (**Fig. 2a,**
111 **Supplementary Fig. 4a**). When those ZsGreen^{+} BMDMs were sorted for imaging by high-resolution

spinning disk confocal microscopy, we readily visualized internalized submicron-sized ZsGreen^{+} puncta (**Fig. 2b-c; Extended Data Fig. 2a**).

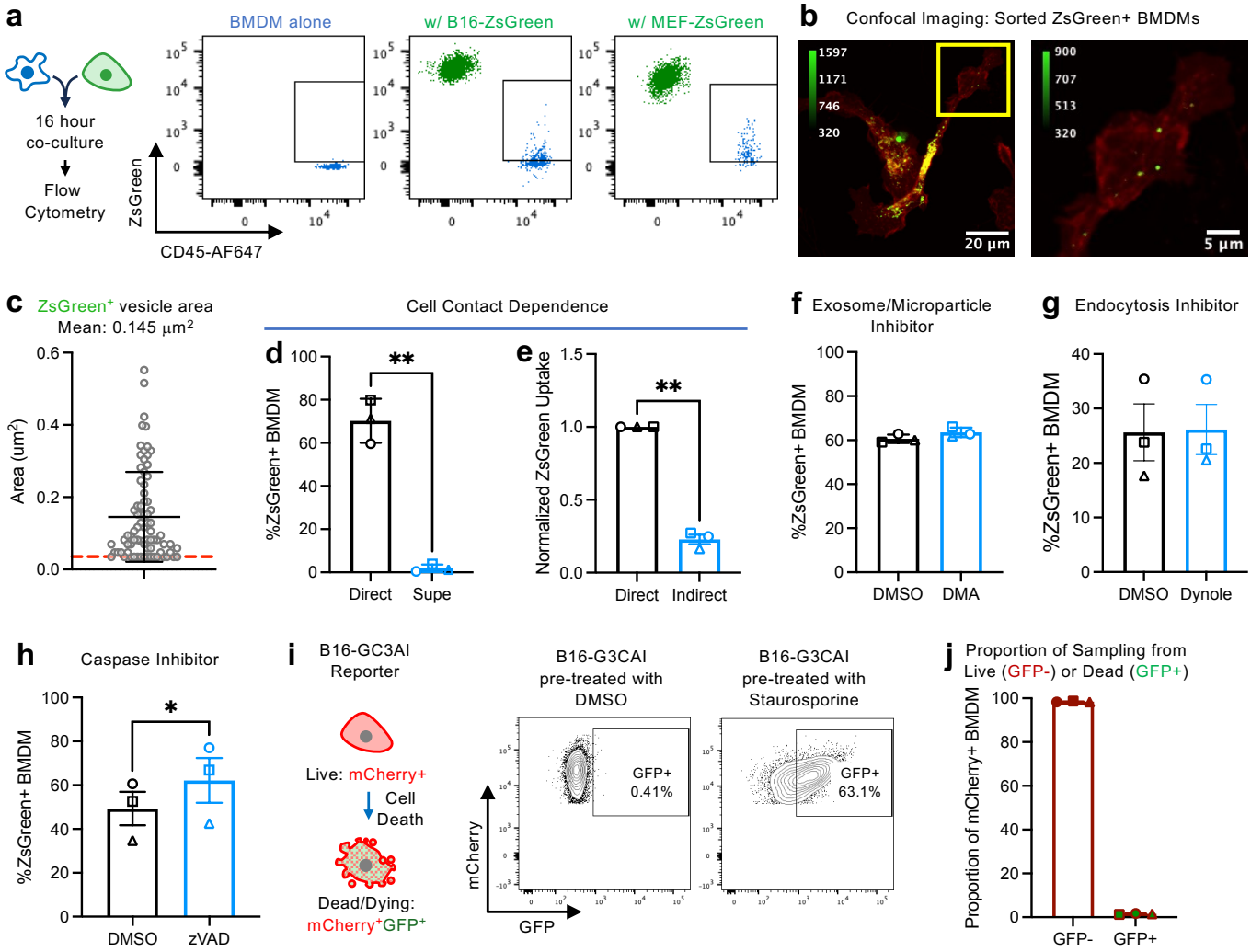

Figure 2: Live cells can be sampled in a cell-contact dependent manner without caspase activation
a, BMDMs and ZsGreen-target cells are co-cultured for 16 hours prior to evaluation for ZsGreen uptake by flow cytometry. **b**, Sorted ZsGreen^{+} BMDMs with membrane Tomato showcasing ZsGreen^{+} puncta .(**c**) Area of individual ZsGreen^{+} vesicles. n = 77 vesicles quantified from 23 cells. Shown are mean +/- s.d. **d-e**, BMDMs were co-cultured directly with B16s ("Direct"), with B16 supernatant (**d**, "supe"), or with a transwell insert containing B16s (**e**, "Indirect")). **f-h**, In vitro co-cultures were treated with indicated inhibitors or DMSO vehicle control. **i,** Induction of GFP in B16-F10 expressing GFP caspase 3 activity indicator (B16-GC3AI) treated with DMSO or Staurosporine. **j**, BMDM co-culture with B16-GC3AI demonstrates uptake is predominantly from live mCherry^{+}GFP^{-} target cells. n = 3 biological replicates. Shown are mean of technical replicates +/- s.e.m. Two-sided paired t-test. * $p < 0.05$, ** $p < 0.01$. MEF, mouse embryonic fibroblast.

We then evaluated whether antigen sampling from live cells in this setting is mediated through uptake of soluble particles and/or was cell-contact dependent, where the former in particular is expected for the ingestion of free exosomes and perhaps apoptotic blebs. Culture of BMDMs with either B16-ZsGreen derived supernatant containing the limited number of exosomes produced in a 48-hour period or B16-

130 ZsGreen cells that were separated from the BMDM by a transwell both significantly reduced uptake (**Fig.**
131 **2d, e; Extended Data 2b**). Additionally, treatment of cultures with inhibitors of either
132 exosome/microparticle release or endocytosis both did not reduce uptake (**Fig. 2f, g; Extended Data 2c-f;**
133 **Supplementary Fig. 4b, c**). Therefore, although endocytosis of soluble material such as exosomes and
134 microparticles may contribute modestly, this suggested a distinct dominant mechanism of uptake of live
135 cell-associated material in this setting, requiring cell-contact.
136
137 Since an existing paradigm suggests that phagocytosis of apoptotic bodies, termed efferocytosis but
138 heretofore just "phagocytosis", is the major mechanism by which tissues donate material to surveilling
139 APCs[15–17], we sought to test whether cell death is necessary for the substantial sampling in our system.
140 When we treated the co-culture with the caspase inhibitor zVAD, we found no effect upon ZsGreen uptake,
141 a result which does not support that this uptake relies on cell death (**Fig. 2g**, **Extended Data Fig. 2f,g;**
142 **Supplementary Fig. 4d**). To study more directly whether the material ingested into macrophages came
143 from cells undergoing apoptosis, we used a B16-F10 model cell line expressing constitutive mCherry and
144 a split GFP caspase 3 activity indicator which fluoresces only when cleaved, as during apoptosis[18] ("B16-
145 GC3AI") (**Fig. 2i**). Use of this confirmed that the B16-GC3AI cells that went into our assays were highly
146 viable (0.12% GFP^+), whereas apoptotic cell death induced by Staurosporine resulted in GFP reporter
147 fluorescence (>63% GFP, **Fig. 2i**). When these reporter-expressing cells were co-cultured with BMDM, we
148 found that the majority of the mCherry-positive cells (those that had taken up material from the donor cells)
149 lacked GFP expression compared to uptake following apoptosis (1% for live sampling**,** versus 11%
150 following staurosporine; **Fig. 2j, Extended Data Fig. 2h)**. Together, these results further support that an
151 alternative sampling pathway, beyond those involving apoptosis, exists for obtaining material from live
152 cells.
153
154

155 **Live-Imaging of Live-sampling**

156 Given the small size of particles we found within macrophages, we adopted high-resolution methods to
157 directly image the time-course of B16-ZsGreen cells interacting with BMDMs expressing membrane-
158 TdTomato in a co-culture. We variously used lattice light sheet imaging with isotropic resolution of
159 approximately ~220nm, or the Nikon Spatial Array Confocal (NSPARC), detector system which utilizes an
160 ultra-low noise detector array with approximate lateral and axial resolutions of approximately ~212nm and
161 ~424nm, respectively. Importantly, both technologies can sample live full cell volumes over time with
162 reduced phototoxicity.

163

164 Using NSPARC, we observed target cell-BMDM interactions that spontaneously result in the stretching of
165 a protrusion of the target cell into the BMDMs. This was frequently followed by the separation of a distinct
166 ZsGreen^{+} vesicle (**Fig. 3b**). In a representative movie (**Fig. 3b, Supplementary Movie 1**), this entire
167 process took <10 minutes from imaging of the initial ZsGreen^{+} protrusion until the time when a protrusion
168 was no longer visible from the target cell, although we registered the actual abscission of the vesicle within
169 a single frame (30 seconds; **Fig. 3a, b**) followed by complete loss of the remaining tether, either into the
170 vesicle or back into the donor cell. We confirmed, at the end of the process, that very small amounts of
171 target cell material were physically inside the BMDM by analyzing the same data in YZ and XZ projections
172 (**Extended Data Fig. 3a**). Consistent with the size ranges we have observed in vivo[13], these separated
173 vesicles were small, ranging from diffraction limited (<~0.02μm^3) to ~0.05μm^3 (**Fig. 3c**). In some cases,
174 we also saw a protrusion pulled into the BMDM but then retracted without detectable pinching of a vesicle,
175 which might either have led to extremely tiny ingestion or was simply abortive. Post-ingestion, ZsGreen^{+}
176 puncta moved within the cytoplasm (**Extended Data Fig. 3b**). These data suggest that live-cell cytosolic
177 material can be sampled in a contact-dependent, trogocytosis-like manner.

178

179 To confirm that this process was not an artefact of the detection method and to take advantage of faster
180 frame-rates, we also leveraged lattice light sheet (LLS) microscopy[19] with its isotropic high resolution,
181 which again captured the stretching and separation of ZsGreen^{+} vesicles, this time again visible across a
182 single frame (now ~8 seconds; **Fig. 3d, Extended Data Fig. 3d, Supplementary Movie 2**). Although
183 ingested vesicles were occasionally identified using spinning disk confocal (**Extended Data Fig. 3c**), it is
184 possible that the small size of these vesicles (limiting total fluorescent yield) and the lower sampling rate
185 of this ingestion method limits our ability to capture this biology with older technologies. This also provides
186 one possible explanation why this process has not yet been described or extensively studied by conventional
187 microscopic methods.
188

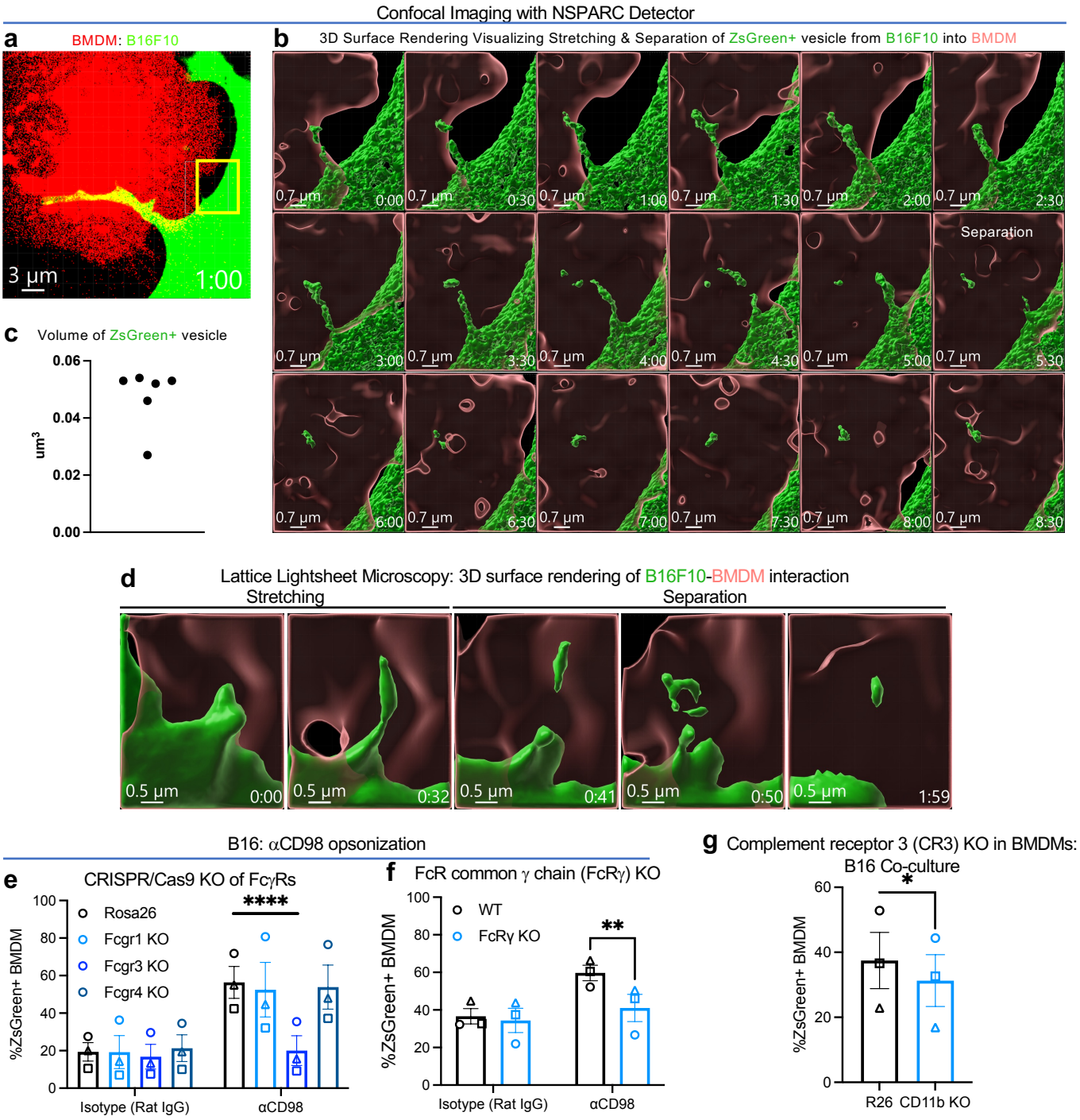

Figure 3: Trogocytosis-like sampling enables macrophages to ingest cytosolic protein from live cells

a-b, Confocal live imaging of TdTomato$^+$ BMDM and ZsGreen$^+$ B16F10 interactions using the NSPARC detector. Time shown as m:ss. **a,** Two-color volume rendering displaying interaction between TdTomato$^+$ BMDM and ZsGreen$^+$ B16F10. Yellow box highlights the region of interest displayed in **(b). b,** Three-dimensional surface rendering from ROI in **(a)** visualizing the formation and separation of a vesicle from ZsGreen+ B16 into TdTomato+ BMDM. Z-stacks within series were captured in 30 sec intervals. **c,** Volume measurements of separated vesicles from frames 13-18 in **(b)** using Imaris object statistics. **d,** Lattice light-sheet imaging of TdTomato$^+$ BMDM and ZsGreen$^+$ B16F10 capturing the stretching and separation of ZsGreen$^+$ vesicle from target cell. Time shown as m:ss. **e-f,** Antibody-opsonized B16-ZsGreen target cells were co-cultured with either **(e)** BMDMs targeted at the *Rosa26* control locus or receptor loci using CRISPR-Cas9 RNP or **(f)** BMDMs isolated from wild-type B6 mice or FcRγ KO mice. **g**, BMDMs targeted at the *Rosa26* control locus or *Itgam* locus encoding CD11b were co-cultured with B16-ZsGreen target cells. n = 3 biological replicates. Shown are mean +/- s.e.m. Two-way ANOVA with Sidak's multiple comparison or two-sided paired t-test. * $p < 0.05$, ** $p < 0.01$, **** $p < 0.0001$.

204 **Receptor-mediated mechanisms mediate sampling from live cells**

205 Although multiple receptor-ligand interactions are likely to contribute to this process, we first asked whether
206 previously described mechanisms such as antibody-opsonization or complement receptor 3 (CR3)
207 engagement couple facilitate sampling from live cells. To this end, we found that, pre-incubation with
208 antibodies to surface protein CD98 increased ZsGreen uptake (**Fig. 3f**). Consistent with previously reported
209 binding specificity of Rat IgG1κ to Fcγ receptor 3 (FcγR3, CD16)[20], this enhancement required FcγR3
210 binding and signaling (**Fig. 3f-i, Extended Data Fig. 4a-c**). Pre-incubation with antibodies to another
211 abundant surface protein, CD29, similarly increased uptake in an FcγR-dependent manner (**Extended Data**
212 **Fig. 4d-f**). Moreover, pre-incubation of ZsGreen target cells with normal mouse serum or isolated IgG prior
213 to co-culture with BMDMs increased ZsGreen uptake (**Extended Data Fig. 4g,h),** suggesting that even
214 weakly cross-reactive collections of antibodies amplifies sampling from live cells. Furthermore, we found
215 that disruption of complement receptor CR3 (CD11b) in BMDM decreases the frequency and intensity of
216 ZsGreen uptake in B16 and MEFs (**Fig. 3h, Extended Data Fig. 5a-c**), similar to findings that synaptic
217 pruning by microglia involves these receptors[21].

218

219 Next, to identify other surface proteins beyond CD11b and FcγR involved in this process, we used
220 NicheNet[22] to predict ligand-receptor interactions between our two model target cells and BMDMs
221 (**Extended Data Fig. 5d**). Because CD11b also has established roles in phagocytosis, we prioritized shared
222 receptors with known phagocytic functions[23], confirmed their protein, and evaluated their contribution to
223 ZsGreen uptake. Of the eight candidate receptors that we examined, only KO of CD93, a C-type lectin
224 receptor, showed a modest but significant decrease in ZsGreen uptake (**Extended Fig. 5e-g**). These results
225 indicate that multiple surface interactions contribute to uptake, with CD11b and CD93 playing partial roles.

226

227 We next examined signaling pathways that link receptor engagement to uptake using small-molecule
228 inhibitors. We targeted signaling downstream of CD11b (Src, Syk, PI3K), small GTPases important for

229 vesicle trafficking (Arf6, Cdc42, Rac), and actin nucleation proteins (Arp2/3, formins). Inhibiting Src
230 signaling (PP1), PI3K signaling (GDC-0941), and Arp2/3 (CK-666) decreased but did not completely
231 abrogate uptake (**Extended Data Fig. 6**). These results suggest that receptor mediated activation of Src and
232 PI3K, leading to Arp2/3-driven branched actin assembly, supports vesicle formation. In contrast, Syk, small
233 GTPases, and formin-driven linear actin may be dispensable or redundant in our system. Altogether, these
234 data indicate that pleiotropic mechanisms contribute to this contact-dependent sampling process that
235 nevertheless relies on local activation cues at the cell-cell interface.
236

237 **Tracking sampled material using high-dimensional intracellular vesicle flow cytometry**

238 We sought to determine whether this mechanism has any distinct functional downstream consequences for
239 the vesicle or cargo by first interrogating its fate as compared to material obtained by phagocytosis or
240 endocytosis. To facilitate a high-dimensional analysis of the organelles that derived from different modes
241 of cell sampling, we developed a 10-parameter flow-based organelle profiling method, loosely based on a
242 previous phagoFACS[24], here capable of immunophenotyping of multiple intracellular compartments (**Fig.**
243 **4a**, see **Methods**). Importantly, we incorporated a cell-surface biotinylation step prior to lysis, to allow
244 definitive discrimination of surface-derived membrane, and we also stained the preparation with amine-
245 binding CellTraceViolet to focus analysis upon protein-associated intracellular organelles (**Fig. 4b**,
246 **Supplementary Fig. 5a,** see **Methods**). Reassuringly, markers for intracellular organelles such as Early
247 Endosome Antigen 1 (EEA1) and RAB7 are exclusively detected in the streptavidin-negative material (**Fig.**
248 **4c**). In CellTraceViolet^{+} intracellular vesicles isolated from BMDMs, we were able to distinguish ZsGreen^{+}
249 antigen-containing vesicles from ZsGreen^{-} antigen-free vesicles, and these were exclusively found in
250 BMDMs that had been co-cultured with ZsGreen-expressing target cells (**Fig. 4d, Supplementary Fig. 5b**).
251

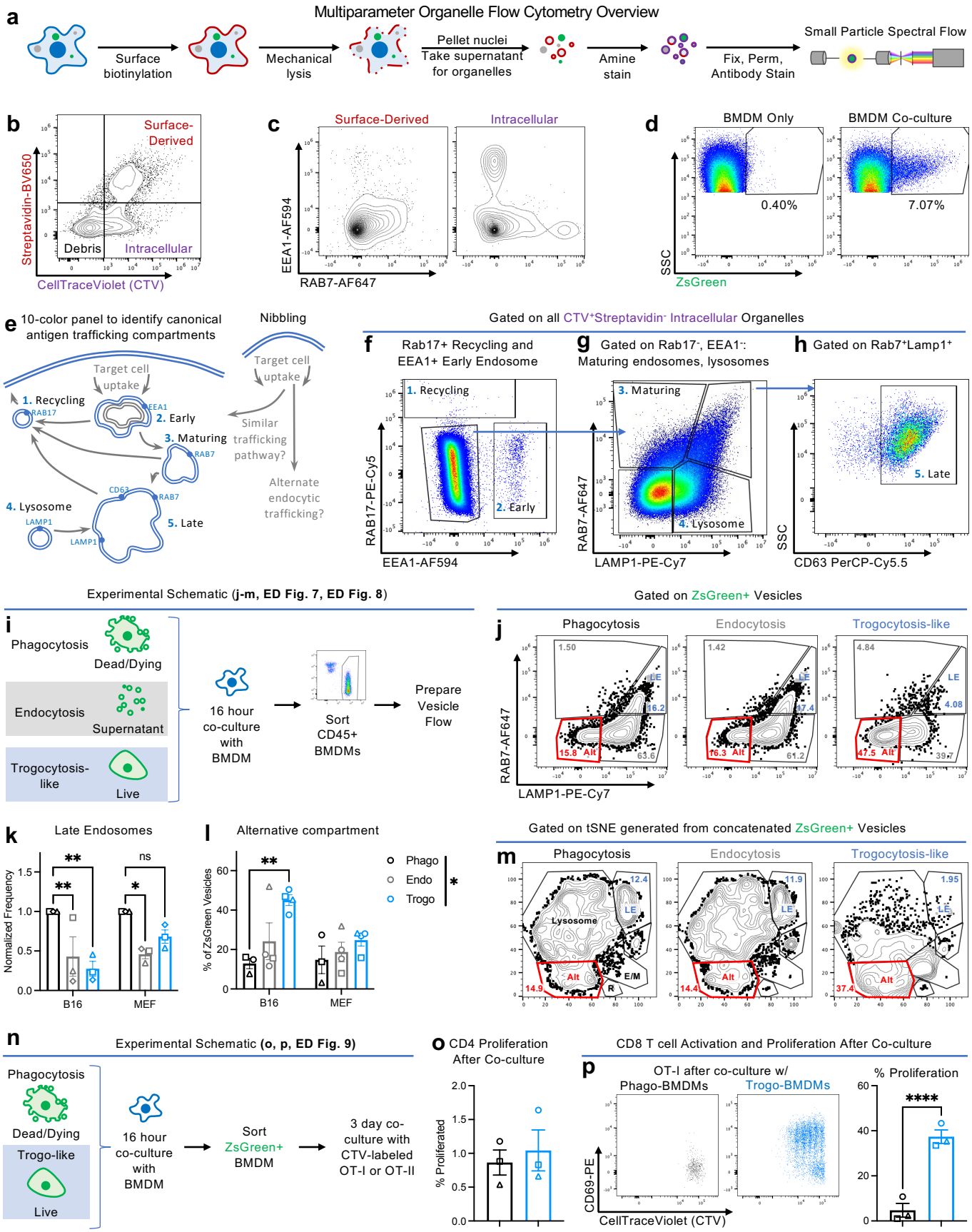

Figure 4: Multiparameter intracellular vesicle flow cytometry reveals that live-cell associated protein fills a discrete vesicular compartment

a, Cell surface membrane is biotinylated prior to mechanical lysis and low-speed centrifugation. Supernatant containing organelles are stained with CellTraceViolet, fixed, permed, and stained with antibodies against vesicle-associated antigens. **b,** Discrimination of Strepavidin^{-} CellTraceViolet^{+} intracellular, protein-containing particles. **c,** Vesicle-staining antibodies primarily stain intracellular particles. **d,** Discrimination of ZsGreen+ vesicles allows for tracking of vesicles containing target-cell-derived protein. **e-h,** Identification of vesicle compartments by vesicle flow panel. **i,** Experimental schematic to evaluate trafficking downstream of different sampling mechanisms. **j-m,** Representative flow plots (**j**) or tSNE (**m**) of ZsGreen^{+} vesicles derived from different sampling mechanism with summary quantification of proportion of ZsGreen^{+} vesicles in late endosome (**k**) and alternative compartment (**l**). **n,** Experimental schematic to evaluate T cell activation downstream of different sampling mechanisms. ZsGreen^{+} BMDMs were sorted after co-culture with live or apoptotic B16F10-ZsGreen-minOVA target cells and subsequently co-cultured with CellTraceViolet (CTV)-labeled OT-I CD8+ or OT-II CD4+ T cells in a 1:3 BMDM:T ratio for 3 days. **o,** Proliferation of OT-II CD4 T cells as read out by loss of CellTraceViolet after 3 days of co-culture with ZsGreen+ BMDMs that ingested material using phagocytosis (black) or trogocytosis-like (blue) mechanisms. **p,** Activation and proliferation of OT-I CD8 T cells as read out by CD69 expression or loss of CellTraceViolet after 3 days of co-culture with ZsGreen+ BMDMs from phagocytosis (black) or trogocytosis (blue) conditions. n = 3-4 biological replicates. Shown are mean of technical replicates +/- s.e.m. Two-way ANOVA with Dunnett's multiple comparisons test or two-sided paired t-test. * $p < 0.05$, ** $p < 0.01$, **** $p < 0.0001$. LE, late endosome; Alt, alternative compartment; E/M, early/maturing endosomes; R, recycling endosomes.

Vesicles derived from internalization are understood to flow through a pathway consisting of progressively more degradative compartments; early endosomes mature into late endosomes that fuse with lysosomes to form phagolysosomes[10,25]. We tuned our panel to identify known vesicular compartments, including RAB17^{+} recycling endosomes, EEA1^{+} early endosomes, LAMP1^{+} lysosomes, RAB7^{+} maturing endosomes, and RAB7^{+}LAMP1^{+}CD63^{+} late endosomes (**Fig. 4e-h**). By further incorporating antibodies recognizing antigen presentation molecules major histocompatibility complex (MHC) I and II, we could identify compartments consistent with antigen-loading. Consistent with previous reports[10], MHC I is primarily excluded from LAMP1^{+} vesicles whereas MHC II can be detected across multiple vesicular compartments (**Extended Data 7a-b**). Together, these results highlighted the suitability of a high-dimensional vesicle analytic method to study composition and identity of vesicular compartments.

We then applied this organelle immunophenotyping method to compare the intracellular trafficking of ZsGreen^{+} antigen-containing vesicles after trogocytosis-like live-sampling to other sampling mechanisms, including endocytosis and phagocytosis (**Fig. 4i**). While endocytosis of soluble material derived from supernatant resulted in very low levels of ZsGreen uptake, sufficient ZsGreen vesicles were nevertheless detectable for downstream analysis (**Extended Data Fig. 7c-d**). In a conventional gating analysis, both phagocytosis and endocytosis resulted in distributions of proteins across the vesicle maturation spectrum,

290 but revealed decreased trafficking of vesicles resulting from trogocytosis-like sampling to the late endosome
291 (**Fig. 4j,k, Extended Data Fig. 7e-f**) and target cell-dependent changes in the co-localization of these with
292 MHC-I but not MHC II (**Extended Data Fig. 7g**). Notably, while ~90% of ZsGreen^{+} vesicles resulting
293 from phagocytosis were associated with a conventional vesicle marker, a substantial portion of ZsGreen+
294 vesicles resulting from live-sampling did not associate with these canonical endocytic markers (**Fig. 4l**).
295 This suggested the sequestration of live-sampled material into an alternative endocytic trafficking pathway,
296 rather than those associated with degradation.
297
298 To analyze vesicle populations based on their intensity for each of our markers and in a way unbiased by
299 previous classifications, we displayed the concatenated ZsGreen^{+} vesicles in a t-distributed stochastic
300 neighbor embedding (tSNE) plot using only the vesicle protein marker intensities as parameters (**Extended**
301 **Data Fig. 8a,b**). This demonstrated that while vesicles derived from each sampling method overlapped,
302 there was a distinct shift in the distribution of vesicles comparing live-sampling (trogocytosis-like), to
303 conventional phagocytosis of apoptotic cells (**Fig. 4m, Extended Data Fig. 8b**). When we overlayed
304 intensities of markers such as LAMP1 and consistent with the conventional flow gating strategy, vesicles
305 resulting from live-sampling were relatively depleted in late endosomes and enriched in an alternative
306 vesicular compartment (**Fig. 4m, Extended Data Fig. 8c**).
307
308 To independently assess lysosomal delivery, we performed confocal microscopy and quantitative co-
309 localization analysis. This confirmed that ZsGreen acquired through live-sampling showed significantly
310 lower overlap with LAMP1 compared to antigen acquired from phagocytosis (**Extended Data Fig. 8d-f**),
311 further supporting that live-cell-derived antigen has a unique vesicular fate.
312
313

314 **Live-sampling biases T cell activation by BMDMs**

315 Immunologically, the nature of sampling may have repercussion for how internalized antigens are presented
316 to T cells on Class I ('cross-presentation') versus Class II MHC. To examine how sampling through this
317 trogocytosis-like mechanism affects antigen presentation, we isolated ZsGreen^{+} BMDMs after co-culture
318 with DMSO- or Staurosporine-treated B16F10 cell expressing ZsGreen fused to the OT-I and OT-II
319 ovalbumin (OVA) peptides (B16-ZsGminOVA)[13] (**Fig. 4n, Extended Data Fig. 9a**). We detected only
320 weak and indistinguishable activation in OT-II CD4 T cell activation after co-culture with BMDMs that
321 had acquired antigen through phagocytosis ("Phago-BMDMs") compared to those that had sampled live
322 cells ("Trogo-BMDMs") (**Fig. 4o, Extended Data Fig. 9b**). In contrast, Trogo-BMDMs but not Phago-
323 BMDMs induced significant OT-I CD8 T cell proximal activation (CD69 upregulation) and proliferation
324 (**Fig. 4p, Extended Data Fig. 9c**). This is consistent with the absence of trafficking of live-sampled material
325 to the degradative late endosome and lysosomal compartments and suggests a bias for cross-presentation.

326

327 Trogocytosis resulting in trans-cellular membrane transfer (cross-dressing) and T cell activation has been
328 described in dendritic cells[26]. To determine if this is occurring in our system, we performed antigen transfer
329 and T cell stimulation assays using Balb/c-derived BMDMs (**Extended Data Fig. 9d**). MHC-I allele H2Kb
330 was undetectable on either Balb/c BMDMs cultured alone or ZsGreen^{+} Balb/c BMDMs that had ingested
331 material from B16-ZsGreen-minOVA target cells (**Extended Data Fig. 9e**). Consistent with this, ZsGreen^{+}
332 Balb/c BMDMs induced significantly less antigen-specific CD8 T cell proliferation compared to ZsGreen^{+}
333 B6 controls (**Extended Data Fig. 9f**). Thus, while limited peptide-MHC transfer may occur, the majority
334 of CD8 T cell activation must be due to BMDM processing and presentation of ingested cytosolic antigen.

335

336 **Redirecting antigen to the lysosome is associated with decreased T cell activation**

337 Material ingested through clathrin-, dynamin-independent mediated endocytosis is diverted away from
338 lysosomal degradation[27], and the SNX27-retromer complex can prevent lysosomal delivery of ingested

339 material[28] (**Fig. 5a**). Because live-sampling in our system is likewise dynamin-independent and leads to
340 non-degradative trafficking, we examined how disrupting SNX27 affects antigen trafficking and ensuing T
341 cell responses. CRISPR-Cas9-mediated targeting of the *Snx27* locus in BMDMs introduced indels and
342 decreased protein expression at high efficiency (**Fig. 5b,c**). SNX27 KO did not impair ZsGreen sampling
343 (**Extended Data Fig. 10a**). However, compared to *Rosa26*-targeted controls, SNX27 KO increased
344 ZsGreen trafficking to LAMP1^{+} lysosomes and reduced the fraction of ZsGreen in the alternative
345 compartment (**Fig. 5d,e, Extended Data Fig. 10b**), consistent with live-sampled material being diverted
346 from the lysosome downstream of live-sampling.
347
348 To determine whether these trafficking changes were associated with loss of cross-presentation, we co-
349 cultured SNX27 KO or control BMDMs with B16-ZsGreen-minOVA target cells and isolated ZsGreen+
350 BMDMs for co-culture with OT-I CD8 T cells. Consistent with increased antigen degradation, SNX27 KO
351 BMDMs induced less T cell proliferation (**Fig. 5f**). Importantly, SNX27 KO did not impair T cell
352 proliferation when BMDMs were pulsed with SL8 peptide (**Extended Data Fig. 10c**), confirming that the
353 effect is due to altered antigen processing rather than general defects in APC functionality.

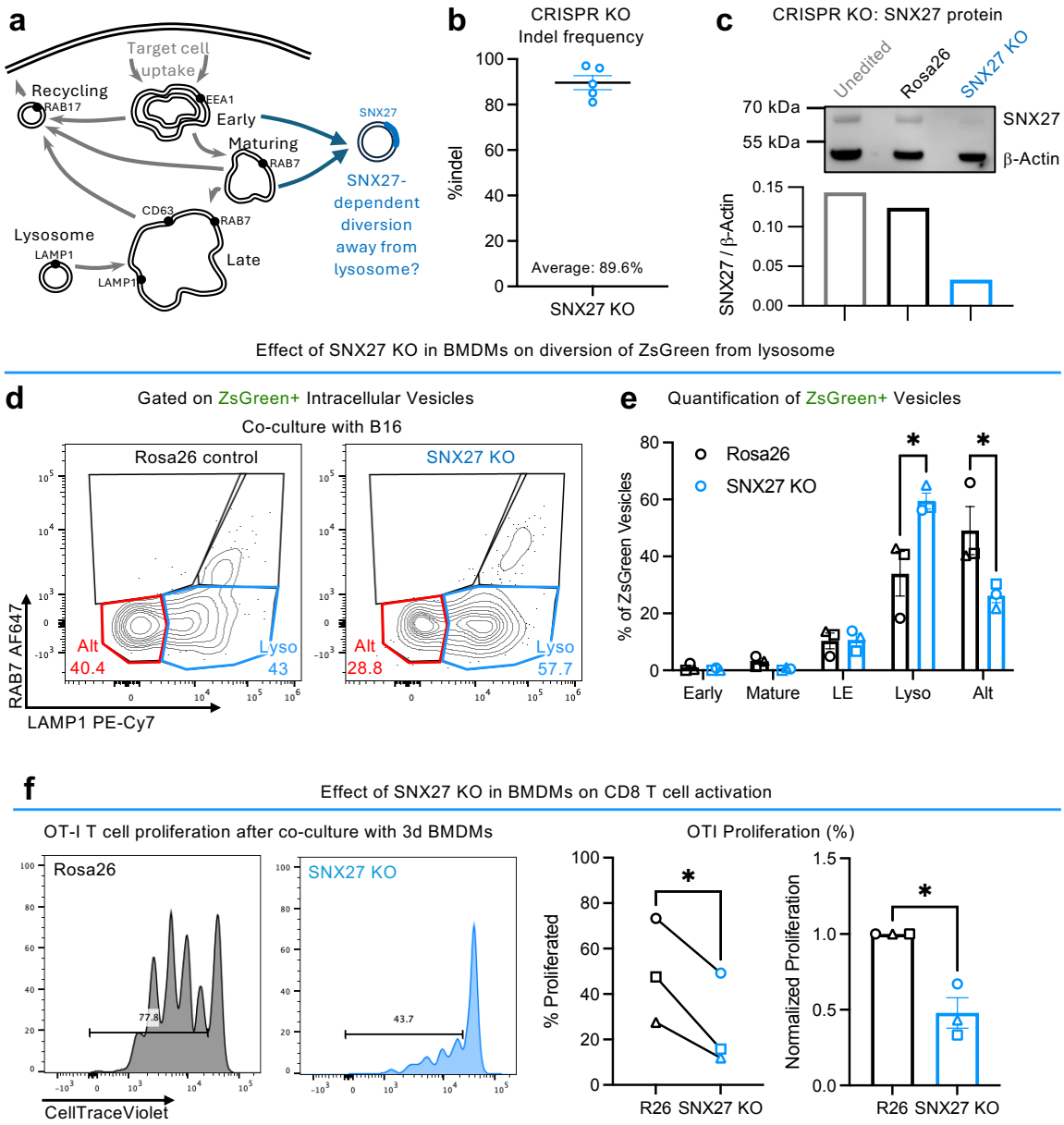

Figure 5: SNX27 KO in macrophages increases antigen trafficking to lysosomes and decreases CD8 T cell activation
a, Schematic illustrating SNX27-dependent diversion of material away from lysosomal maturation into alternative endocytic pathways. **b-c**, Validation of SNX27 KO in BMDMs by (**b**) indel quantification by ICE analysis (mean +/- s.d.) and (**c**) western blot (representative of 2 experiments). β-Actin was probed on the same gel as a loading control. For gel source data, see **Supplementary Fig. 1**. **d-e**, CRISPR-Cas9-targeted BMDMs were co-cultured with ZsGreen target cells to evaluate ZsGreen trafficking. **f**, OT-I CD8 T cell proliferation after 3-day co-culture with FACS-isolated ZsGreen^{+} *Rosa26*-targeted and SNX27 KO BMDMs that live-sampled B16-ZsGreen-minOVA target cells. n = 3-5 biological replicates. Shown are Shown are mean +/- s.e.m unless otherwise specified. Two-tailed paired t-test or two-way ANOVA with Sidak's multiple comparison. *, $p < 0.05$

364 **DISCUSSION**

365 Together, these findings demonstrate a substantial sampling of live cells that takes place via a trogocytosis-
366 like mechanism and which fills a distinct vesicular compartment that are particularly underrepresented in
367 late endosomes[10]. That macrophages can constitutively ingest small amounts of material from live cells is
368 in itself unsurprising; indeed a pruning function for macrophages has been demonstrated to be important to
369 activate stem cells[29] and to optimize brain circuitry via small synaptic pruning[30]. A key distinction here is
370 in revealing that a very low-volume trogocytosis-like sampling may be ongoing at steady state in a variety
371 of cells and may be a significant source of self-antigen from healthy cells, giving macrophages a distinct
372 endocytic trafficking mechanism with which to present healthy-self antigens, notably to CD8 T cells. We
373 also note a single previous suggestion of trogocytosis by dendritic cells which focused on a more
374 conventional 'ripping' mechanism leading to direct transfer of pre-formed peptide-MHC from the donor
375 cell membrane[26]. In contrast, using previously unavailable vesicle cytometry, our studies highlight the
376 maintenance of sampled material in a depot that can be processed by the APC for presentation. A more
377 stable depot of self-antigens provides a means of integrating and presenting the self-identity of many
378 sampled cells, perhaps over days or longer. The longer retention of material sampled by this trogocytosis-
379 like mechanism may contribute to a transferable pool of these vesicles, as have been observed to be
380 exchanged amongst myeloid cells[13]. While we use model antigen and transgenic T cells in our study to
381 reveal the capability of macrophages to cross-present live-cell-associated antigen by stimulating T
382 proliferation, the functional role of this cross-presentation for maintaining or tuning homeostatic T cell
383 populations that have undergone thymic self-tolerance requires further investigation. Ultimately, this work
384 provides a novel framework to understand how the immune system can accumulate information about our
385 healthy-self: a system that then can tune T cells to the normal concentrations of self-protein but may also
386 be exploited by tumor cells to promote pathologic outcomes.

387

388 **Acknowledgments:** We thank all members of the Krummel lab, Jayanta Debnath, Caleb R. Glassman,
389 and Graham Barlow for discussion and support. We acknowledge the UCSF Parnassus Flow Core CoLabs,
390 particularly Vinh Nguyen and Tamara Roach, for assistance generating flow cytometry data (RRID:
391 SCR_018206; DRC Center Grant NIH P30 DK063720) and the Biological Imaging Development Colab
392 with assistance in data collection, instrumentation, and processing (NIH shared equipment grant
393 S10OD028611-01). pCDH-puro-CMV-GC3AI was a gift from Binghui Li (Addgene plasmid # 78910;
394 http://n2t.net/addgene:78910; RRID:Addgene_78910). FcRγ KO mice were a gift from Dr. Oscar Aguilar.
395 We thank Tristan Courau for providing the custom anti-TREM2 antibody. This work was supported by
396 R01 AI175277-01 and 2 R01 CA197363-06A1 to MFK. A.C.F. was supported by T32HL007185 and the
397 A.P. Giannini Postdoctoral Research Fellowship and Leadership Award. R.T. was supported by
398 T32AI007334. N.S. was supposed by the Human Frontier Science Program (LT000061/2018-L). V.S.V.
399 was supported by the UCSF Medical Scientist Training Program (T32GM141323) and the Achievement
400 Rewards for College Scientists scholarship. M.K.R was supported by the Cancer Research Institute
401 Irvington Postdoctoral Fellowship.
402

403 **Author contributions:**

404 A.C.F. and M.F.K. conceived the study, with N.S. contributing to initial conception. Methodology was
405 developed by A.C.F., with N.S., and M.K.R. contributing to the initial methodological framework.
406 Investigation was performed by A.C.F. (antigen transfer assays, imaging collection, imaging analysis,
407 inhibitor studies, vesicle flow cytometry, T cell co-culture assays, indel analysis), R.T. (antigen transfer
408 assays, imaging analysis, T cell co-culture assays), N.S. (in vivo experiments, imaging collection), V.S.V.
409 (indel analysis, western blot, T cell co-culture assays), K.M. (imaging collection), M.K.R. (in vivo
410 experiments, imaging collection), L.L. (antigen transfer assays), G.J. (cell isolation), and A.E (imaging
411 analysis). Formal analysis was carried out by A.C.F. and R.T. Data curation was performed by A.C.F.

Visualization was carried out by A.C.F., R.T., and N.S. A.C.F. wrote the original draft, and R.T. and M.F.K. reviewed and edited the manuscript. M.F.K. supervised the study and acquired funding.

Declaration of Interests: Authors declare no competing interests.

Supplementary Information is available for this paper.

418 **METHODS**

419 **RESOURCE AVAILABILITY**

420 ***Lead Contact***

421 Further information and requests should be directed to the Lead Contact: Matthew F. Krummel
422 (matthew.krummel@ucsf.edu).

423

424 ***Materials Availability***

425 Requests for resources and reagents should be directed to and will be fulfilled by the Lead Contact:
426 Matthew F. Krummel (matthew.krummel@ucsf.edu).

427
428 **EXPERIMENTAL MODEL AND SUBJECT DETAILS**
429

430 **Mice**

431 Mice were housed and bred under specific pathogen-free conditions at the University of California, San
432 Francisco Laboratory Animal Research Center and all experiments conformed to ethical principles and
433 guidelines approved by the UCSF Institutional Animal Care and Use Committee, the National Institutes of
434 Health and the American Association of Laboratory Animal Care. C57BL/6 (RRID: MGI:2159769), Ai16[31]
435 ("mTmG"), B6;129P2-Fcer1g^{tm1Rav}/J[32] ("FcRγ KO", RRID: MGI:2162818), and Balb/c (RRID:
436 MGI:2161072) mice were purchased from Jackson Laboratory or bred in house. Both male and female mice
437 ranging in age from 6 to 20 weeks were used for experimentation. Food and water were provided ad libitum.

438

439 To generate ZsGreen reporter mice, Ai6 mice were crossbred with K14-Cre, Scgb1a1-Cre-ERT2, Villin-
440 Cre, B-actin-Cre mice. To induce ZsGreen expression in Scgb1a1-Cre-ERT2;Ai6 mice, mice were fed
441 tamoxifen-containing chow ad libitum for two weeks.

442

443 For tumor studies, B16-F10 melanoma cancer cells were resuspended in PBS and mixed at a1:1 (v:v) ratio

444 with growth factor reduced Matrigel Matrix (BD Biosciences) and 100000 cells in 50 uL were transplanted
445 into the subcutaneous region of the mouse flank. On day 14 after tumor challenge, when tumors reached a
446 size/volume of approximately 0.5 cm^3, mice were sacrificed, tumors were excised and processed for
447 downstream analysis.
448
449 **Tumor cell lines**
450 B16-F10 (ATCC, CRL-6475) was purchased. B16ZsGreen and B16ZsGreen minOVA cell lines were
451 described previously[13]. In brief, to make this cell line, B16-F10 melanoma parental cells were genetically
452 engineered using viral transduction with a ZsGreen or ZsGreen-minOVA construct. B16-GC3AI cell lines
453 were genetically engineered to stably express the GFP-Casp3-activity-indicator using viral transduction
454 with AddGene construct (Addgene #78910). Adherent cell lines were cultured at 37° C in 5% CO_2 in
455 DMEM (Invitrogen), 10% FCS (Benchmark), Pen/Strep/Glut containing 2 mM L-glutamine, 100 U/ml
456 penicillin, and 100 mg/ml streptomycin (Invitrogen).
457
458 **Mouse embryonic fibroblasts**
459 Mouse embryonic fibroblasts (MEFs) were derived from Ai6;B-actinCre mice that were generated by
460 crossing B-actin-Cre (strain # 033984, The Jackson Laboratory) to Ai6 mice (strain # 007906,The Jackson
461 Laboratory) as previously described[33]. Briefly, day 13.5 embryos were collected from pregnant females,
462 were minced, and digested with Trypsin. The retrieved cells were washed and plated in DMEM
463 (Invitrogen), 15% FCS (Benchmark), Pen/Strep/Glut (Invitrogen) for overnight culture at 37° C in 5% CO_2.
464 Media was aspirated after 24 h to remove any cells remaining in suspension and replaced with fresh media.
465 Cells were then grown to 70%–80% confluency and cryopreserved.
466
467

468 **METHOD DETAILS**

469 **Tissue digest and flow cytometry staining**

470 *Lung*

471 Lungs were collected from mice following euthanasia by overdose with 2.5% Avertin. Lungs were placed
472 in 3 mL of DMEM (Gibco) in C-Tubes (Miltenyi) briefly processed with a GentleMACS Dissociator
473 (Miltenyi). 2 mL of DMEM with 0.26 U/mL LiberaseTM (Roche) and 0.25 mg/mLDNase I (Roche) was
474 subsequently added and samples were then incubated at 37° C in a shaker for 30 min and dissociated to
475 single cell suspensions by GentleMACS. Tissue homogenate was then passed through a 100 mm filter. Red
476 blood cells were lysed with 3 mL of RBC Lysis Buffer (155 mM NH4Cl, 12 mM NaHCO3, 0.1 mM EDTA)
477 per lung for 5 min at room temperature. Samples were then washed with FACS buffer (2% FBS, 2mM
478 EDTA in PBS) and resuspended in appropriate buffer for staining for flow cytometry or FACS.

479

480 *Tumor*

481 For tumor digests, tumors from mice were harvested 14 days after injection. Tumors were minced and
482 incubated in digestion buffer (100 U/mL collagenase type I (Roche), 500 U/mL collagenase type IV
483 (Roche), and 200 mg/mL DNAse I (Roche) in RPMI1640 (Gibco)) for 30 minutes on a shaker at 37 ^{o} C.
484 Digestion mixtures were then pipetted repeatedly, followed by a second 15-minute incubation at 37° C.
485 Cells were quenched with RPMI-1640 (GIBCO) plus 10% FCS, washed with FACS buffer, and filtered
486 through a 100-mm cell strainer before staining for flow cytometry.

487

488 *Lymph Nodes*

489 Inguinal lymph nodes (LN) were dissected from mice, cleaned of fat, and digested as previously described
490 [14]. In brief, LN were pierced and torn with sharp forceps in 24-well plates and incubated for 15 min at 37°
491 C in 1 ml digestion buffer (100 U/ml collagenase type I (Roche), 500 U/ml collagenase type IV (Roche),
492 and 20 μg/ml DNAse I (Roche) in RPMI-1640 (GIBCO)). Cells were pipetted up and down repeatedly,

493 followed by a second 15-minute incubation at 37° C. After digestion, LN were washed with RPMI-1640
494 (GIBCO) plus 10% FCS, washed with FACS buffer, and filtered through 70 μm Nytex filters before staining
495 for flow cytometry.
496

497 **Imaging Sample Preparation, Image Acquisition, and Image Analysis**

498 *Two photon imaging of mouse lung, skin, tumor, and gut slices.*

499 Imaging of lung, skin, tumor, and gut slices were performed using a custom-built two-photon setup
500 equipped with two infrared lasers (MaiTai: Spectra Physics; Chameleon: Coherent). The Chameleon laser
501 was set to 950nm for excitation of ZsGreen. Emitted light was detected using a 25x 1.2NA water lens
502 (Zeiss) coupled to a 6-color detector array (custom; using Hamamatsu H9433MOD detectors). Emission
503 filters used were blue 475/23, green 510/42, yellow 542/27, red 607/70, far red 675/67. The microscope
504 was controlled by the MicroManager software suite, and time-lapse z stack images were acquired every 90
505 s with five-fold averaging and z-step of 4mm. Data analysis was performed with Imaris software (Bitplane).
506 For lung slices, mice were euthanized by anesthetic overdose with 1 mL 2.5% Avertin and then
507 intubated by tracheotomy with the sheath from an 18-gauge i.v. catheter. Lungs were subsequently inflated
508 with 1 mL of 2% low melting agarose (BMA) in sterile PBS at 37C. Agarose was then solidified by flooding
509 the chest cavity with 4C PBS. Inflated lungs were excised, and the left lobe was cut into 300mm sections
510 using a vibratome. For skin, tumor, and gut slices, mice were euthanized using CO2, obstructing fat was
511 removed, and tissue sections were embedded in 4% low-melting agarose in PBS prior to sectioning.
512 Sections were mounted on plastic coverslips and imaged by two-photon microscopy at 37C in carbogen
513 (5% CO2:95% O2)-perfused RPMI-1640 media (GIBCO, without Phenol Red) in a heated chamber.
514

515 *Spinning Disk Confocal*

516 Glass bottom 96 well plates were coated in fibronectin and washed as described above. BMDMs, sorted
517 ZsGreen^{+} BMDMs after antigenic transfer, or unsorted antigenic transfer assays were imaged. Live imaging

518 by spinning disk confocal was performed at 37°C with a 488 and 561 nm lasers with 40% and 50% laser
519 powers, respectively. For LAMP1 staining, cells were fixed with 4% PFA at room temperature for 15
520 minutes, permeabilized with 0.5% saponin at room temperature for 15 minutes, incubated with blocking
521 buffer (1% BSA, 0.1% saponin, 5% normal rat serum) at room temperature for 60 minutes, and incubated
522 at LAMP1-AF647 in blocking buffer at 4C overnight. Fixed cells were imaged with 488 and 640 at 25%
523 laser powers.
524
525 *Nikon NSPARC*
526 Glass bottom 96 well flat bottom plates were coated with 50ug/mL fibronectin in H_2O at 37°C for 1 h, or
527 at 4°C overnight, before use. Fibronectin coated wells were washed 2x with PBS prior to use. $8x10^3$
528 $TdTomato^+$ BMDMs were plated with $1.2x10^4$ ZsGreen+ B16F10s or ZsGreen+ MEFs and spun at 1500g
529 for 5 min. Cells were incubated at 37°C for 2 hours prior to imaging. NSPARC imaging was performed at
530 37°C with 488 and 560 nm lasers with 1.0% and 2.0% laser powers, respectively.
531
532 *Lattice light-sheet microscopy*
533 5 mm round coverslips were cleaned by a plasma cleaner and coated with 2 µg/ml fibronectin in H_2O at
534 37°C for 1 h, or at 4°C overnight, before use. Fibronectin coated coverslips were washed 2x with PBS prior
535 to use. Cells were plated onto fibronectin-coated coverslips 20 min prior to imaging with a 10 min spin at
536 1,400 rpm and 4°C. Coverslip was immediately loaded into the sample bath with warmed imaging media
537 and secured. Imaging was performed at 37°C with a 488 and 560 nm laser (MPBC). Exposure time was 10
538 ms per frame leading to a temporal resolution of ~4.5. LLS microscope was a homebuilt clone of the scope
539 described by Chen et al.[34] with a Nikon CFI Apo LWD 25× W 1.1 NA 2 mm working distance objective,
540 Hamamatsu Orca Flash 4.0 v2 camera, and Custom LabView acquisition software. Method was derived
541 from previous work[19].
542

543 *Image Analysis*

544 All computational image analysis was performed in Imaris version 9.9.1 or 10.2.0 (Bitplane) and Fiji
545 version 2.16.0/1.54p. Particle area analysis was performed using the Analyze particles function in Fiji with
546 the following parameters: size (.027- infinity) and circularity (0.00-1.00). Post processing raw data from
547 lattice light-sheet images were deconvoluted using iterative Richardson-Lucy deconvolution as
548 implemented in LLSpy. Briefly, images were deconvolved with a known point spread function that was
549 recorded for each color prior to the experiment, as described previously[19]. A typical sample area underwent
550 15-20 iterations of deconvolution. For live imaging experiments, photobleaching correction was applied in
551 FIJI using the histogram matching method. Particle volume was measured using the object-object statistics
552 function in Imaris from the separated vesicle in frames 13-18.

553

554 For ZsGreen colocalization analysis with LAMP1, Mander's coefficients were calculated using the JACoP
555 plugin on ImageJ[35]. Otsu thresholding was used to identify optimal thresholding for the phagocytosis
556 condition. To account for the low fluorescence intensities of ZsGreen vesicles in the live sampling
557 condition, we opted for a manual threshold level of 550. Thresholding results were confirmed by comparing
558 to ZsGreen negative BMDMs.

559

560 **Flow cytometry and fluorescence-activated cell sorting**

561 Zombie NIR Fixable Viability Kit (#423106; BioLegend), DAPI, or PI was used for exclusion of dead cells.
562 Surface staining was performed with anti-mouse Fc receptor antibody (clone 2.4G2, UCSF Hybridoma
563 Core) in FACS buffer for 30 min on ice. Supplementary Table 1 lists all antibodies referenced for flow
564 cytometry and imaging experiments. Apoptotic cells were detected by staining with Annexin V AF647
565 (Biolegend #649012) and 1μg/mL DAPI in Annexin V binding buffer (Biolegend #422201). For all
566 experiments involving intracellular staining, BD Cytofix/Cytoperm (#554722) was used. Following fixation
567 and permeabilization, cells were incubated with Fc block for 10 min on ice prior to addition of intracellular

568 stain. Flow cytometry was performed on a BD Fortessa instrument, and sorting was performed on BD
569 FACSAria or BD FACSAria Fusion instruments. FlowJo software (BD Biosciences) was used for all
570 analyses.
571
572 **Generation of BMDMs**
573 6-12 week old C57BL/6 mice were euthanized and their femurs and tibiae were excised. Bone marrow was
574 crushed using a mortar and pestle. After pelleting the bone marrow, the red blood cells were lysed using
575 RBC lysis buffer for 5 min at RT. Cells were washed with FACS buffer and filtered through a 100 mm cell
576 strainer before being seeded at 1x106 cells / mL on a low-adherent cell culture dish in BMDM media
577 (DMEM supplemented with 10% FBS (Benchmark), 50 mM beta-mercaptoethanol, Pen/Strup/Glut
578 (Invitrogen), and 20 ng/ml M-CSF (Peprotech)). Fresh BMDM media was added on day 3-4 of culture. On
579 day 6-7 of culture, BMDMs were harvested and used for experiments.
580
581 **In vitro antigen transfer assay**
582 BMDMs were isolated as described above and co-cultured with target B16-ZsGreen cells or MEF-ZsGreen
583 cells at a 1:1 ratio for 16 hours before assays unless otherwise noted. Cells were plated in BMDM media in
584 TC-treated 96 well flat-bottom plates prior to staining and analysis by flow cytometry.
585
586 **Drug/Inhibitor antigenic transfer assay**
587 Antigenic transfer assays were performed as described above. For all experiments wherein apoptosis was
588 induced, B16F10 cells or MEFs were treated with 1μM Staurosporine (Tocris Bioscience, Cat# 1285) and
589 washed with PBS prior to antigenic transfer assays. For exosome/microparticle inhibitory experiments, 5-
590 (N,N-Dimethyl)amiloride hydrochloride (DMA, Sigma Aldrich, Cat# A4562) was plated at 0 h to a final
591 concentration of 10μM. For endocytic inhibition experiments Dynole 34-2 (Cayman Chemical Company
592 #34073) was plated at 0 h to a final concentration of 5μM. Caspase inhibition was performed using zVAD-

593 FMK (Invivogen, Cat # tlrl-vad) at a final concentration of 20μM for B16-ZsGreen or 30μM for MEF-
594 ZsGreen at 0 h. Signaling and cytoskeleton inhibition was performed using 10 μM PP1 (Cayman #14244),
595 5 μM Piceatannol (MedChemExpress #HY-13518), 10 μM GDC-0941 (Selleck Chemicals #S1065), 1.35
596 μM NAV-2729 (MedChemExpress #HY-112473), 25 μM NSC23766 (MedChemExpress #HY-15723), 10
597 μM ZCL278 (MedChemExpress #HY-13518), 200 μM CK-666 (Sigma-Aldrich #SML0006-5MG), or 5
598 μM SMIFH2 (MedChemExpress #HY-16931).
599

600 **Drug/Inhibitor functional validation and cell toxicity validation**

601 For exosome/microparticle inhibitor validation, target cells were cultured with DMA and supernatant was
602 collected to quantify ZsGreen^{+} vesicles by small particle flow cytometry. For endocytosis inhibitor
603 validation, exosomes were isolated from confluent B16-ZsGreen cultures using the ExoQuick kit (System
604 Biosciences #EXOA5A-1), and BMDMs were cultured with exosomes and Dynole 34-2 or DMSO control.
605 Exosome endocytosis was quantified with flow cytometry. For apoptosis inhibition studies, B16-ZsGreen
606 or MEF-ZsGreen target cells were pre-treated with zVAD for 1 hour prior to Staurosporine treatment.
607 %AnnexinV^{+}DAPI$^{+/-}$ apoptotic cells were evaluated by flow cytometry. For toxicity studies, cells were
608 treated with drug or vehicle control for 16 hours and quantified by flow cytometry with CountBright beads
609 (Invitrogen #C36950).
610

611 **Supernatant/transwell antigenic transfer assay**

612 Media was replaced on B16-ZsGreen cells or MEF-ZsGreen cells upon reaching 80% confluency. After 48
613 hours, supernatants were collected and used in antigenic transfer assays as described above. Transwell
614 experiments were performed as described in antigen transfer assays with a 3μm pore transwell insert
615 separating BMDM and ZsGreen+ target cells or supernatants.
616

617 **Antibody Opsonization and Blockade**

618 For opsonization experiments, B16-ZsGreen or MEF-ZsGreen target cells were pre-coated with 10ug/mL
619 Armenian Hamster IgG (BD Pharmigen, Cat# 553969), 10µg/mL Rat IgG2ak (clone 2A3, invivoMab Cat#
620 BE0089), 10µg/mL CD29 (eBioHmb1-1, eBioscience Cat #16-0291-85), 10µg/mL aCD98 (RL388,
621 Biolegend Cat# 128202), normal mouse serum (Jackson ImmunoResearch Cat# 015-000-120), or
622 500µg/mL IgG from normal mouse serum at 37C for 30-60 minutes and washed with PBS prior to co-
623 culture with BMDMs. IgG from normal mouse serum was isolated using Protein G dynabeads (Invitrogen
624 Cat# 10003D) according to manufacturer instructions and dialyzed with PBS (Slide-A-Lyzer).
625 Concentration of isolated IgG was quantified using IgG ELISA (abcam, Cat # ab151276).
626 For antibody blockade, BMDMs were pre-treated with 10µg/mL Rat IgG2b (clone MPC-11, invivoMab
627 Cat# BE0086), CD16/32-blocking antibody (clone 2.4G2), CD11b-blocking antibody (clone M17/0,
628 Biolegend Cat# 101202, RRID: AB_312785), CD49e blocking antibody (clone 5H10-27(MRF5),
629 Biolegend Cat# 103801, RRID: AB_313050), SIRPα blocking antibody (Clone P84, Biolegend Cat#
630 144035, RRID: AB_2832516), or custom afucosylated mouse IgG2a monoclonal blocking antibody against
631 TREM2 (provided by Tristan Courau, synthesized by Evitra) for 1 hour before 16-hour co-culture antigen
632 transfer assays.
633
634 **CRISPR Editing of Primary BMDMs**
635 CRISPR editing of primary BMDMs were performed as previously described[36]. Briefly, sgRNA targeting
636 *Rosa26 (ACUCCAGUCUUUCUAGAAGA)*, *Fcgr1* (*GAUCACCUUGCAGCCUCCAU*), *Fcgr3*
637 (*UGGUGAAACUGGACCCCCCA*), *Fcgr4* (*GGUGAACCUAGACCCCAAGU*), *Itgam*
638 *(GAAGCCAUGACACAAGGCUA)*, *Itgav* (*UUGAAUCAAACUCAAUGGGC*,
639 *CCUGUUGAAUCAAACUCAAU*), *Tlr2* (*UUGGCUCUUCUGGAUCUUGG*), *C5ar1*
640 (*CAUGGAUCCUAACAUACCUG*, *GAUCCUAACAUACCUGCGGA*, *AUGGCAUUCACCUCCCGAAG*),
641 *Cd93* (*CAGGAACAAACCAGUUGAGA*, *AGAAGAAUGGCCAUCUCAAC*,
642 *CUGGUUUGUUCCUGCUGCUG*), and *SNX27* (*GGAACGGCGUGAAUGUUGAG*,

643 *UGAGGGGGCGACACACAAGC*, *GUGGUGGACCUGAUCCGAGC*) were ordered from Synthego or IDT
644 and reconstituted to 100uM in TE (IDT). sgRNA and Cas9 (6.5mg/mL) was complexed in a 2:1 molar ratio
645 at room temperature for at least 10 minutes. At 3 days after initial plating, BMDM differentiation cultures
646 were harvested, and cells were washed with PBS prior to electroporation with ribonucleoprotein (RNP)
647 containing gene-targeting sgRNA complexed in P3 primary cell solution with electroporation code CM137
648 using the Lonza 4D Nucleofector. After an additional 4 days of differentiation, gene-edited BMDMs were
649 either stained with antibodies for validation of protein knockdown or co-cultured with ZsGreen target cells
650 for 16 hours before evaluated by flow cytometry. For indel quantification with ICE, DNA was extracted
651 with QuickExtract for PCR of the targeted locus with Phusion Plus Green PCR Master Mix (Thermo
652 Scientific #F632S) and primers (5' *CCCCATCTTTCCCACATGCT* 3', 5' *ATTACTGTAGGCCACCCCCT*
653 3').
654
655 **NicheNet analysis to predict receptors**
656 To identify potential BMDM surface proteins mediating live-sampling using NicheNet[22], we used the
657 BMDM datasets from Johannessen, *et al*[37], B16 dataset from Griffin, Wu, Iracheta-Vellve, *et al*[38], and MEF
658 dataset from Jaber, *e al*[39]. The BMDM was set as the "receiver" population and B16/MEF were set as sender
659 populations. A threshold for expressed genes for each population was defined based on Gaussian fit of gene
660 expression BMDM receptors were prioritized if predicted to interact with both cell types, overlap with
661 known phagocytic modulators, and confirmed to be expressed at the protein level.
662
663 **Vesicle Flow Cytometry**
664 *Sample Preparation and Sorting*
665 16 hours prior to sorting, BMDMs were cultured with live target cells ("Trogocytosis") in a 1:1 ratio,
666 Staurosporine-treated target cells ("Phagocytosis") in a 1:1 ratio, or supernatant derived from target cells
667 ("Endocytosis"). Cells were harvested, washed with FACS buffer, stained with CD45-BUV395 with

668 FcBlock for 30 minutes on ice, washed with FACS buffer, and resuspended in FACS buffer + 1 mg/mL PI
669 at 10E6 cells/mL. $CD45^+$ cells were sorted on FACSAria and FACSFusion machines on "Purity" into FACS
670 buffer kept at 4C.
671
672 *Surface Biotinylation and Lysis*
673 Cells were washed 3x in PBS, resuspended in PBS at 25E6 cells/mL then biotinylated with 80 uL of 10mM
674 EZ-Link Sulfo-NHS-SS-Biotin (ThermoFischer Scientific #21331) per mL of reaction volume for 30
675 minutes at 4C. Cells were washed 3x in PBS, resuspend in at least 500 μL homogenization buffer (250mM
676 sucrose, 200mM PMSF, 250mM sucrose, 3mM Imidazole, 1X protease inhibitor filtered through 0.1um
677 filter) at a concentration of 10E6 cells/mL, and drawn 15 times up and down through a 22G needle. Cell
678 homogenate was spun for 4 minutes at 150xg, and post-nuclear supernatant was spun at 3000xg for 5 min
679 at 4C to collect vesicles.
680
681 *Staining*
682 All staining reagents were filtered using a 0.1μm filter prior to use and vesicles were pelleted using spin
683 speeds of 3000xg for 5 min at 4C for all steps. Vesicles were stained with 50μM CellTrace Violet
684 (ThermoFischer Scientific Cat# C34557) for 5 minutes at room temperature and washed once with PBS.
685 Samples were fixed for 20 minutes at room temperature with fixation buffer (Invitrogen Cat# 88-8824-00),
686 washed with permeabilization buffer (Invitrogen Cat# 88-8824-00) twice, and stained in 50 μL of
687 permeabilization buffer with 1% FCS with FcBlock for 30 minutes at room temperature. Vesicles were
688 washed with permeabilization buffer and resuspend in 100 μL PBS for acquisition.
689
690 *Sample Acquisition and Analysis*

691 Aurora Cytek flow cells were soaked with contrad overnight with long clean prior to acquisition with
692 filtered reagents. Calibration beads and samples were acquired on the Aurora Cytek with Enhanced Small
693 Particle detection.
694
695 **T cell stimulation assays**
696 ZsGreen^{+} BMDMs were sorted from BMDM 16-hour co-cultures with DMSO- or Staurosporine-pretreated
697 B16zsGreenminOVA. To induce MHC II expression on BMDMs, sorted cells were stimulated with
698 20ng/mL IFNγ for 2 hours and then washed prior to co-culture with T cells. OTI and OTII T cells were
699 isolated from spleens of TCR transgenic mice after RBC lysis using either a CD8 or CD4 EasySep
700 enrichment kit (STEMCELL Technologies), respectively. T cells were labeled with CellTraceViolet
701 (ThermoFischer Scientific) at 37C in PBS for 15 minutes and washed in RPMI prior to use. T cell
702 stimulation assay was performed as previous described. Briefly, sorted BMDMs and T cells were added to
703 the wells of a 96-well V-bottom plate at a 1:3 ratio in RPMI (Gibco) supplemented with 10% FCS
704 (Benchmark), Pen/Strep/Glut (Invitrogen), and 50 mM beta-mercaptoethanol (Thermo Fisher). Cells were
705 harvested for analysis 3 days later. Dilution of cell permeable dye CellTraceViolet and expression of CD69
706 were used as indicators of T cell stimulation.
707
708 **Western Blot**
709 Whole-cell protein lysates were obtained from BMDMs in Pierce RIPA buffer [Thermo Scientific, Cat#
710 89901] and ProteoGuard EDTA-Free Protease Inhibitor Cocktail (Takara, Cat# 635673). Lysates were
711 extracted via sample agitation at 4°C for 30 minutes, followed by 4°C centrifugation at 16,000 RPM for 20
712 minutes. Protein concentration was determined with Pierce BCA Protein Assay Kit (Thermo Fisher).
713 Lysates were denatured in NuPage LDS sample buffer (Invitrogen, Cat# NP0007) supplemented with
714 NuPAGE Sample Reducing Agent (Invitrogen, Cat# NP0009) by incubation at 95°C for 5 minutes.
715 Denatured samples were loaded onto a NuPAGE 10% (Cat# NP0302BOX) or 4% to 12% Bis-Tris (Cat#

716 NP0323BOX) polyacrylamide gel (Thermo Fisher) with PageRuler Plus Prestained Protein Ladder
717 (Thermo Scientific, Cat#26619) and electrophoresed in MES running buffer (Invitrogen). Gels were
718 transferred to PVDF membranes with the iBlot 2 system (Invitrogen, Cat# IB21001), blocked with Pierce
719 Clear Milk Blocking Buffer (Thermo Scientific, Cat# 37587), and incubated with primary antibodies
720 according to the manufacturers' directions. Primary antibodies, SNX27 (Abcam, Clone: EPR218130-16,
721 Cat# ab315897), and β-Actin (Invitrogen, Cat #PA1-183, RRID: AB_2539914) were detected with Goat
722 Anti-Rabbit IgG HRP-conjugated secondary antibodies (Southern Biotech, Cat# 4050-05, RRID:
723 AB_2795955) and SuperSignal West Femot Maximum Sensitivity Substrate (Thermo Scientific, #34095).
724 Membranes were imaged with the Licor Odyssey XF system.
725

726 **QUANTIFICATION AND STATISTICAL ANALYSIS**

727 **Statistical analysis**

728 Unless specifically noted, all data are representative of >3 separate experiments. Experimental group
729 assignment was determined by genotype or, if all WT mice, by random designation. Statistical analyses
730 were performed using GraphPad Prism software. Error bars represent standard error of the mean (S.E.M.)
731 calculated using Prism, and are derived from triplicate or greater experimental conditions. Specific
732 statistical tests used were paired and unpaired t-tests and p values <0.05 were considered statistically
733 significant. For pairwise comparisons, unpaired t tests were used unless otherwise noted. For statistical
734 measures between more than two groups, one-way ANOVA would be performed unless otherwise noted.
735 Investigators were not blinded to group assignment during experimental procedures or analysis.
736

737 **DATA AVAILABILITY**

738 The data reported are in the Article and its associated Supplementary, and all relevant data are available
739 from the corresponding author on request. Source data are provided with this paper. Transcriptomic data
740 were downloaded from NCBI GEO database, accession numbers GSE99759, GSE155972, and

741 GSE171127.

742 **REFERENCES**

743 1. Medawar, P.B. (1961). IMMUNOLOGICAL TOLERANCE.

744 2. Goodnow, C.C., Sprent, J., de St Groth, B.F., and Vinuesa, C.G. (2005). Cellular and genetic mechanisms of self tolerance
745 and autoimmunity. Nature *435*, 590–597. https://doi.org/10.1038/nature03724.

746 3. Kamradt, T., and Mitchison, N.A. (2001). Tolerance and Autoimmunity. N. Engl. J. Med. *344*, 655–664.
747 https://doi.org/10.1056/NEJM200103013440907.

748 4. Kenison, J.E., Stevens, N.A., and Quintana, F.J. (2023). Therapeutic induction of antigen-specific immune tolerance. Nat.
749 Rev. Immunol., 1–20. https://doi.org/10.1038/s41577-023-00970-x.

750 5. Cummings, R.J., Barbet, G., Bongers, G., Hartmann, B.M., Gettler, K., Muniz, L., Furtado, G.C., Cho, J., Lira, S.A., and
751 Blander, J.M. (2016). Different tissue phagocytes sample apoptotic cells to direct distinct homeostasis programs. Nature *539*,
752 565–569. https://doi.org/10.1038/nature20138.

753 6. Kushwah, R., Wu, J., Oliver, J.R., Jiang, G., Zhang, J., Siminovitch, K.A., and Hu, J. (2010). Uptake of apoptotic DC
754 converts immature DC into tolerogenic DC that induce differentiation of Foxp3+ Treg. Eur. J. Immunol. *40*, 1022–1035.
755 https://doi.org/10.1002/eji.200939782.

756 7. Myers, D.R., Zikherman, J., and Roose, J.P. (2017). Tonic Signals: Why do Lymphocytes Bother? Trends Immunol. *38*,
757 844–857. https://doi.org/10.1016/j.it.2017.06.010.

758 8. Stefanová, I., Dorfman, J.R., and Germain, R.N. (2002). Self-recognition promotes the foreign antigen sensitivity of naive
759 T lymphocytes. Nature *420*, 429–434. https://doi.org/10.1038/nature01146.

760 9. Hogquist, K.A., and Jameson, S.C. (2014). The self-obsession of T cells: how TCR signaling thresholds affect fate
761 "decisions" and effector function. Nat. Immunol. *15*, 815–823. https://doi.org/10.1038/ni.2938.

762 10. Blum, J.S., Wearsch, P.A., and Cresswell, P. (2013). Pathways of Antigen Processing. Annu. Rev. Immunol. *31*, 443–473.
763 https://doi.org/10.1146/annurev-immunol-032712-095910.

764 11. Greene, J.T., Brian, B.F., Senevirathne, S.E., and Freedman, T.S. (2021). Regulation of myeloid-cell activation. Curr.
765 Opin. Immunol. *73*, 34–42. https://doi.org/10.1016/j.coi.2021.09.004.

766 12. White, S.R. (2011). Apoptosis and the Airway Epithelium. J. Allergy *2011*, 948406. https://doi.org/10.1155/2011/948406.

767 13. Ruhland, M.K., Roberts, E.W., Cai, E., Mujal, A.M., Marchuk, K., Beppler, C., Nam, D., Serwas, N.K., Binnewies, M.,
768 and Krummel, M.F. (2020). Visualizing Synaptic Transfer of Tumor Antigens among Dendritic Cells. Cancer Cell *37*, 786-
769 799.e5. https://doi.org/10.1016/j.ccell.2020.05.002.

770 14. Roberts, E.W., Broz, M.L., Binnewies, M., Headley, M.B., Nelson, A.E., Wolf, D.M., Kaisho, T., Bogunovic, D.,
771 Bhardwaj, N., and Krummel, M.F. (2016). Critical Role for CD103+/CD141+ Dendritic Cells Bearing CCR7 for Tumor
772 Antigen Trafficking and Priming of T Cell Immunity in Melanoma. Cancer Cell *30*, 324–336.
773 https://doi.org/10.1016/j.ccell.2016.06.003.

774 15. Pham, T., Mero, P., and Booth, J.W. (2011). Dynamics of Macrophage Trogocytosis of Rituximab-Coated B Cells. PLOS
775 ONE *6*, e14498. https://doi.org/10.1371/journal.pone.0014498.

776 16. Blander, J.M. (2017). The many ways tissue phagocytes respond to dying cells. Immunol. Rev. *277*, 158–173.
777 https://doi.org/10.1111/imr.12537.

778 17. Yin, C., and Heit, B. (2021). Cellular Responses to the Efferocytosis of Apoptotic Cells. Front. Immunol. *12*.
779 https://doi.org/10.3389/fimmu.2021.631714.

780 18. Zhang, J., Wang, X., Cui, W., Wang, W., Zhang, H., Liu, L., Zhang, Z., Li, Z., Ying, G., Zhang, N., et al. (2013).
781 Visualization of caspase-3-like activity in cells using a genetically encoded fluorescent biosensor activated by protein cleavage.
782 Nat. Commun. *4*, 2157. https://doi.org/10.1038/ncomms3157.

783 19. Cai, E., Marchuk, K., Beemiller, P., Beppler, C., Rubashkin, M.G., Weaver, V.M., Gérard, A., Liu, T.-L., Chen, B.-C.,
784 Betzig, E., et al. (2017). Visualizing dynamic microvillar search and stabilization during ligand detection by T cells. Science
785 *356*, eaal3118. https://doi.org/10.1126/science.aal3118.

786 20. Wang, Y., Krémer, V., Iannascoli, B., Goff, O.R.-L., Mancardi, D.A., Ramke, L., de Chaisemartin, L., Bruhns, P., and
787 Jönsson, F. (2022). Specificity of mouse and human Fcgamma receptors and their polymorphic variants for IgG subclasses of
788 different species. Eur. J. Immunol. *52*, 753–759. https://doi.org/10.1002/eji.202149766.

789 21. Hong, S., Beja-Glasser, V.F., Nfonoyim, B.M., Frouin, A., Li, S., Ramakrishnan, S., Merry, K.M., Shi, Q., Rosenthal, A.,
790 Barres, B.A., et al. (2016). Complement and microglia mediate early synapse loss in Alzheimer mouse models. Science *352*,
791 712–716. https://doi.org/10.1126/science.aad8373.

792 22. Browaeys, R., Saelens, W., and Saeys, Y. (2019). NicheNet: modeling intercellular communication by linking ligands to
793 target genes. Nat. Methods. https://doi.org/10.1038/s41592-019-0667-5.

794 23. Cockram, T.O.J., Dundee, J.M., Popescu, A.S., and Brown, G.C. (2021). The Phagocytic Code Regulating Phagocytosis of
795 Mammalian Cells. Front. Immunol. *12*. https://doi.org/10.3389/fimmu.2021.629979.

796 24. Hoffmann, E., Pauwels, A.-M., Alloatti, A., Kotsias, F., and Amigorena, S. (2016). Analysis of Phagosomal Antigen
797 Degradation by Flow Organellocytometry. BIO-Protoc. *6*. https://doi.org/10.21769/BioProtoc.2014.

798 25. Song, W., Cho, H., Cheng, P., and Pierce, S.K. (1995). Entry of B cell antigen receptor and antigen into class II peptide-
799 loading compartment is independent of receptor cross-linking. J. Immunol. *155*, 4255–4263.
800 https://doi.org/10.4049/jimmunol.155.9.4255.

801 26. Harshyne, L.A., Zimmer, M.I., Watkins, S.C., and Barratt-Boyes, S.M. (2003). A Role for Class A Scavenger Receptor in
802 Dendritic Cell Nibbling from Live Cells. J. Immunol. *170*, 2302–2309. https://doi.org/10.4049/jimmunol.170.5.2302.

803 27. Shafaq-Zadah, M., Dransart, E., and Johannes, L. (2020). Clathrin-independent endocytosis, retrograde trafficking, and
804 cell polarity. Curr. Opin. Cell Biol. *65*, 112–121. https://doi.org/10.1016/j.ceb.2020.05.009.

805 28. Burd, C., and Cullen, P.J. (2014). Retromer: A Master Conductor of Endosome Sorting. Cold Spring Harb. Perspect. Biol.
806 *6*, a016774. https://doi.org/10.1101/cshperspect.a016774.

807 29. Wattrus, S.J., Smith, M.L., Rodrigues, C.P., Hagedorn, E.J., Kim, J.W., Budnik, B., and Zon, L.I. (2022). Quality
808 assurance of hematopoietic stem cells by macrophages determines stem cell clonality. Science *377*, 1413–1419.
809 https://doi.org/10.1126/science.abo4837.

810 30. Weinhard, L., di Bartolomei, G., Bolasco, G., Machado, P., Schieber, N.L., Neniskyte, U., Exiga, M., Vadisiute, A.,
811 Raggioli, A., Schertel, A., et al. (2018). Microglia remodel synapses by presynaptic trogocytosis and spine head filopodia
812 induction. Nat. Commun. *9*, 1228. https://doi.org/10.1038/s41467-018-03566-5.

813 31. Muzumdar, M.D., Tasic, B., Miyamichi, K., Li, L., and Luo, L. (2007). A global double-fluorescent Cre reporter mouse.
814 genesis *45*, 593–605. https://doi.org/10.1002/dvg.20335.

815 32. Takai, T., Li, M., Sylvestre, D., Clynes, R., and Ravetch, J.V. (1994). FcR γ chain deletion results in pleiotrophic effector
816 cell defects. Cell *76*, 519–529. https://doi.org/10.1016/0092-8674(94)90115-5.

817 33. Headley, M.B., Bins, A., Nip, A., Roberts, E.W., Looney, M.R., Gerard, A., and Krummel, M.F. (2016). Visualization of
818 immediate immune responses to pioneer metastatic cells in the lung. Nature *531*, 513–517.
819 https://doi.org/10.1038/nature16985.

820 34. Chen, B.-C., Legant, W.R., Wang, K., Shao, L., Milkie, D.E., Davidson, M.W., Janetopoulos, C., Wu, X.S., Hammer,
821 J.A., Liu, Z., et al. (2014). Lattice light-sheet microscopy: imaging molecules to embryos at high spatiotemporal resolution.
822 Science *346*, 1257998. https://doi.org/10.1126/science.1257998.

823 35. Barbet, G., Nair-Gupta, P., Schotsaert, M., Yeung, S.T., Moretti, J., Seyffer, F., Metreveli, G., Gardner, T., Choi, A.,
824 Tortorella, D., et al. (2021). TAP dysfunction in dendritic cells enables noncanonical cross-presentation for T cell priming. Nat.
825 Immunol. *22*, 497–509. https://doi.org/10.1038/s41590-021-00903-7.

826 36. Freund, E.C., Lock, J.Y., Oh, J., Maculins, T., Delamarre, L., Bohlen, C.J., Haley, B., and Murthy, A. (2020). Efficient
827 gene knockout in primary human and murine myeloid cells by non-viral delivery of CRISPR-Cas9. J. Exp. Med. *217*,
828 e20191692. https://doi.org/10.1084/jem.20191692.

829 37. Johannessen, L., Sundberg, T.B., O'Connell, D.J., Kolde, R., Berstler, J., Billings, K.J., Khor, B., Seashore-Ludlow, B.,
830 Fassl, A., Russell, C.N., et al. (2017). Small-molecule studies identify CDK8 as a regulator of IL-10 in myeloid cells. Nat.
831 Chem. Biol. *13*, 1102–1108. https://doi.org/10.1038/nchembio.2458.

832 38. Griffin, G.K., Wu, J., Iracheta-Vellve, A., Patti, J.C., Hsu, J., Davis, T., Dele-Oni, D., Du, P.P., Halawi, A.G., Ishizuka,
833 J.J., et al. (2021). Epigenetic silencing by SETDB1 suppresses tumour intrinsic immunogenicity. Nature *595*, 309–314.
834 https://doi.org/10.1038/s41586-021-03520-4.

835 39. Jaber, M., Radwan, A., Loyfer, N., Abdeen, M., Sebban, S., Khatib, A., Yassen, H., Kolb, T., Zapatka, M., Makedonski,
836 K., et al. (2022). Comparative parallel multi-omics analysis during the induction of pluripotent and trophectoderm states. Nat.
837 Commun. *13*, 3475. https://doi.org/10.1038/s41467-022-31131-8.

838

Extended Data Figure Legends

Extended Data Figure 1: ZsGreen uptake from tissues is not due to Cre mis-expression.
a, Gut taken from mice expressing ZsGreen under the Villin promoter. Isolation of myeloid cells from Villin-Cre;ZsGreen mice shows uptake in gut in macrophages as well as DCs. **b**, Representative flow (left) or quantification of ZsGreen (right) in lung myeloid cell populations in B6 wildtype mice, Scgb1a1-CreERT2;ZsGreen mice with lung-specific ZsGreen expression, and B-actin-Cre-ZsGreen mice. n = 2-6 mice per condition. **c**, Bone marrow transplant of B6 wildtype mice into B-actin-Cre;ZsGreen expressing mice. Myeloid cells isolated from skin-draining inguinal lymph nodes show ZsGreen sampling. **d**, Intracellular staining for airway specific PLVAP protein in lung (black) compared to splenic (gray) myeloid cell populations with ZsGreen+ lung macrophages (green) enriching for PLVAP signal. Shown are mean +/- standard deviation. Representative of 3 experiments, n = 3-6 mice per experiment. M, macrophage; Neu, neutrophil; Mo, monocyte; mDC2, migratory cDC2; mDC1, migratory cDC1; rDC1, residential cDC1; rDC2, residential cDC2; MoMac, Monocyte/Macrophage.

Extended Data Figure 2: Live cells can be sampled in a cell-contact dependent manner without caspase activation
a, Visualization of ZsGreen (C1) puncta ingested from target cells within membrane Tomato (C2) labeled BMDMs. ZsGreen+ BMDMs were sorted and imaged after co-culture with B16-ZsGreen cells. **b,** BMDMs were co-cultured directly with MEFs, with MEF supernatant, or with a transwell insert containing MEFs. **c-d,** Target cells (**c**) or BMDM-MEF co-cultures (**d**) were treated with DMA or DMSO vehicle control. Extracellular vesicle production in supernatant (**c**) or ZsGreen uptake (**d**) was measured by flow cytometry. **e,** Effect of Dynole on endocytosis of ZsGreen^{+} exosomes by BMDMs. **f,** BMDM-MEF co-cultures were treated with indicated inhibitors or DMSO vehicle control. **g,** Target cells were treated with staurosporine and/or zVAD and AnnexinV^{+}DAPI$^{+/-}$ apoptotic cells were measured with flow cytometry. **h,** BMDM co-culture with B16-F10 expressing GFP caspase 3 activity indicator (B16-GC3AI) demonstrates uptake is predominantly from live cells. n = 3 biological replicates. Shown are mean of technical replicates +/- s.e.m. Paired t-test or one-way ANOVA. * $p < 0.05$, ** $p < 0.01$.

Extended Data Figure 3: A trogocytosis-like process can sample target cell protein
a, Three-dimensional surface renderings from the YZ (left) and XY (bottom right) directions to identify intracellular localization of separated vesicle from same ROI as Fig. 3a, b. **b,** Two-color volume rendering showing interactions between TdTomato+ BMDM and ZsGreen+ B16(left) captured immediately after the series in Fig 3b. Three-dimensional surface renderings(right) of ROIs show separated vesicle trafficking towards the nucleus. Time shown as hh:mm:ss. **c,** Spinning-disk confocal imaging of ZsGreen+ B16 and TdTomato+ BMDM showing ingested ZsGreen+ puncta within BMDMs. Time shown as hh:mm. **d,** Three-dimensional surface rendering from Lattice light-sheet imaging of TdTomato+ BMDM and ZsGreen+ B16

Extended Data Figure 4: Antibody opsonization amplifies live-cell sampling
a, Schematic outlining methods used to block or knock-out (KO) FcγR binding and signaling. **b,** BMDMs targeted at the Rosa26 control locus or receptor loci using CRISPR-Cas9 RNP. **c,** BMDMs were pre-incubated with 10 ug/mL 2.4G2 CD16/32 blocking antibody or Rat IgG2b prior to co-culture with antibody-opsonized B16-ZsGreen target cells. **d-e,** CRISPR-targeted BMDMs (**d)** or BMDMs isolated from B6 wildtype or FcγR KO (**e**) mice were co-cultured with B16-ZsGreen or MEF-ZsGreen target cells pre-coated with antibody. **f-g,** BMDMs co-cultured with B16-ZsGreen pre-coated with serum (**f**), or IgG isolated from mouse serum **(g)**. n = 3 biological replicates. Shown are mean of technical replicates +/- s.e.m. Paired t-test. * $p < 0.05$, ** $p < 0.01$.

Extended Data Figure 5: Knockout of CD11b and CD93 decreases live sampling
a, Representative protein knockdown 4 days after CRISPR/Cas9-mediated gene targeting. **b,** ZsGreen uptake in KO cells compared to Rosa26 (R26) controls. **c,** BMDMs were pre-treated with 1ug/uL IgG2b or

CD11b-blocking antibody for 1 hour before 16-hour co-culture antigen transfer assays. **d,** Schematic outlining strategy to identify potential modulators of live sampling. **e,** BMDMs were co-cultured with B16-ZsGreen or MEF-ZsGreen target cells for 16 hours with 5 ug/mL blocking antibody or the appropriate isotype control prior to flow cytometric analysis of ZsGreen uptake. **f-g** BMDMs targeted at the *Rosa26* control locus or receptor loci using CRISPR-Cas9 RNP and co-cultured with B16-ZsGreen or MEF-ZsGreen target cells for 16 hours prior to flow cytometric analysis of ZsGreen uptake (**f**) and receptor expression (**g**). Shown are mean +/- s.e.m. n = 2-3 experiments per receptor, 2-3 technical replicates per experiment. Kruskal-Wallis test with Dunn's multiple comparisons test. * $p < 0.05$.

Extended Data Fig. 6: Src, PI3K, and Arp2/3 inhibition decreases live sampling

a, Schematic illustrating inhibitors used to target components of receptors-mediated uptake. **b-e,** BMDMs, B16-ZsGreen target cells, and MEF-ZsGreen target cells were cultured alone or co-culture for antigen transfer assay and treated with DMSO control, 10 uM PP1, 5 uM Piceatannol, 10 uM GDC-0941, 1.35 uM NAV-2729, 25 uM NSC23766, 10 uM ZCL278, 200 uM CK-666, or 5 uM SMIFH2 for 16 hours prior to flow cytometry analysis for cell number (**b**) or ZsGreen uptake (**c-e**). Data are normalized to DMSO control and compiled over 3-6 experiments. Shown are mean +/- s.e.m. Kruskal Wallis test and Dunn's multiple comparisons. *, $p < 0.05$; **, $p < 0.01$.

Extended Data Figure 7: Live-cell associated antigen fills a discrete vesicular compartment

a-b, Distribution of MHC I **(a)** and MHC II **(b)** in identified vesicular compartments inclusive of both ZsGreen+ and ZsGreen- vesicles. n = 3-4 biological replicates. Shown are mean of technical replicates +/- s.e.m. **c,** Representative sorting gate and purity check for CD45+ BMDMs from 16-hour co-culture. **d,** Representative ZsGreen+ gating from different vesicle flow preps gated on CellTraceViolet+Streptavidin- intracellular vesicles. **e,** Representative flow cytometry of vesicle populations from phagocytosis, endocytosis, and trogocytosis of B16-ZsGreen or MEF-ZsGreen target cells. **f,** Summary quantification of proportion of ZsGreen+ vesicles in different vesicular compartments. **g,** Proportion of ZsGreen+ vesicles that were either MHC I+ or MHC II+. n = 3-4 biological replicates. Shown are mean of technical replicates +/- s.e.m.

Extended Data Figure 8: Live-cell associated antigen fills a LAMP1-negative vesicular compartment

a, tSNE of concatenated ZsGreen+ vesicles from one experiment demonstrating gating of different vesicular compartments. **b,** Distribution of ZsGreen+ vesicles in derived from different sampling mechanism. **c,** Summary quantification of proportion of ZsGreen+ vesicles in late endosome and alternative vesicular compartment gates by gating on tSNE populations. n = 3-4 biological replicates. Shown are mean of technical replicates +/- s.e.m. **d-f,** Sorted ZsGreen+ BMDMs after co-culture with killed B16-ZsGreen (Phago-BMDM) and live B16-ZsGreen (Trogo-BMDM) were fix, permeabilized, and stained with LAMP1-AF647. Representative images are shown in (**d,e**) and quantification per field of view is shown in (**f**). Phago, n = 24; Trogo, n=96. Two-sided student's t-test or Two-way ANOVA. * $p < 0.05$, ** $p < 0.01$.

Extended Data Figure 9: Macrophages process live-cell associated antigen to affect CD8 T cell activation

a, Representative flow plots showing sorting and purity of ZsGreen+ BMDMs after co-culture with live or apoptotic B16F10-ZsGreen-minOVA target cells. **b-c,** Activation and proliferation of OT-I CD8 T cells (**b**) and OT-II CD4 T cells (**c**) as read out by CD69 expression after 3 days of co-culture with ZsGreen+ BMDMs from phagocytosis (black) or trogocytosis (blue) conditions. **d**, Experimental schematic to evaluate strain specific MHC-I transfer and T cell activation by ZsGreen^{+} B6 or Balbc-derived BMDMs. **e**, H2-Kb expression on B16 ZsGreen-minOVA target cells; ZsGreen+ BMDMs after co-culture with B16 ZsGreen-minOVA cels, and BMDMs cultured alone. **f**, OT-I CD8 T cell proliferation after 3-day co-culture with FACS-isolated ZsGreen+ B6 or Balb/c BMDMs. n = 3 biological replicates with n = 3 technical replicates. Shown are mean of technical replicates +/- s.e.m. Two-sided paired t-test. * $p < 0.05$.

938
939 **Extended Data Fig. 10: SNX27 KO reduces antigen diversion from the lysosome but not uptake or**
940 **presentation capacity**
941 **a-c,** ZsGreen uptake (**a**) and vesicle distribution (**b,c**) in SNX27 KO cells compared to Rosa26 (R26)
942 controls. **d,** OT-I proliferation after 3-day co-culture with peptide-pulsed SNX27 KO and Rosa26 control
943 BMDMs.